

# **DESIGN AND PERFORMANCE ANALYSIS OF A FREE SPACE OPTICAL COMMUNICATION LINK USING LASER SOURCE**

Project Thesis

*Submitted by*

**SANDEEP CHOPRA**

**EE13M023**

*In partial fulfillment of the requirements for the award of the degree*

**MASTER OF TECHNOLOGY**

In

**ELECTRICAL ENGINEERING**

*Specialization in*

**COMMUNICATION SYSTEMS**

*Under the guidance of*

**DR BALAJI SRINIVASAN**



**DEPARTMENT OF ELECTRICAL ENGINEERING**

**INDIAN INSTITUTE OF TECHNOLOGY, MADRAS**

**CHENNAI, INDIA**

**MAY 2015**

## THESIS CERTIFICATE

This is to certify that the thesis titled “**Design and Performance Analysis of a Free Space Optical Communication link using LASER Source**” is a bonafide record of the project work carried out by Sandeep Chopra in the Department of Electrical Engineering, Indian Institute of Technology Madras, in partial fulfillment of the requirements for the award of the degree of Master of Technology in Electrical Engineering. The contents of this thesis, in full or parts have not been submitted to any other institute or university for the award of any degree or diploma.

Dr. Balaji Srinivasan  
Project Guide  
Associate Professor  
Dept of Electrical Engineering  
IIT Madras, 600 036

Place: Chennai

Date: 03<sup>rd</sup> May 2015

## ACKNOWLEDGEMENTS

I express my deepest gratitude and thankfulness to **Dr Balaji Srinivisan**, for his unflinching support and guidance throughout the understanding and development of the project, which enabled me to look ahead and move along the intended course of action in the execution of the project. I also wish to thank **Dr Anil Prabhakar**, for his valuable inputs at the initial stages of the project.

I extend my sincere gratitude to **Dr Harishankar Ramachandran**, HoD Electrical Engineering Dept, for encouraging students to take up challenging technical problems.

I would also like to thank **Dr CR Jeevandoss** at Central Electronic Centre, with a special mention of **Ms Jothilakshmi**, Project Technician at FILL Lab for extending full support and cooperation in designing the Electronics for the project work. I place on record the manufacturing facility made available by the Central Workshop, IIT Madras for precision designing of a robust Receiver structure.

I also extend my earnest appreciation towards **Lt Cdr Ankit Atree**, my colleague and a dear friend, who stood by me at crucial times during the course of the project, without whose physical support and words of encouragement the project would have had to face greater challenges. I also place on record the valuable technical guidance offered by **Prof Subrat Kar**, IIT Delhi at initial stages on the aforesaid subject.

I would like to thank my parents and most importantly, my wife, Neha for giving me the freedom to take decisions in every crucial situation which thereby increased my hope and strength to overcome any difficulty that came my way during the course of my project and academic pursuits at this prestigious institute, which I am utterly proud to be a part of.

Finally, any recognition for this project is courtesy ardent endeavour and never-ending guidance of all the above mentioned people, whose motivation, wisdom and professional excellence encouraged me to live up to the benchmark of near perfection.

**SANDEEP CHOPRA**

# **ABSTRACT**

**KEYWORDS:** Free Space Optical (FSO) Systems; LASER; Wireless Communication system, Atmospheric Turbulence

In the Defence Environment, operations demand secure, relevant and timely information. The ability to relay massive amounts of information is becoming a critical determinant of military success. For this reason, information superiority on the battlefield is one of the prime objectives. Furthermore, the complexity of military missions has also dramatically increased, with more diverse theatres of operation, expanded spectrums of conflict, and a tremendous increase in the requirement for information to be delivered almost immediately to the war fighter. With a very high bandwidth available to FSO systems, use of such a technology could give the military a much greater leverage over its enemy counterparts. Intelligence, Surveillance, and Reconnaissance (ISR) platforms are seen as a major target for FSO technology as these platforms need to disseminate large volumes of sensor, imagery and video to the fighting forces, often in real-time in the fastest and most reliable manner. Secure wireless backhaul solutions is a need of the Hour for today's digitized Battlefield.

This Project entails detailed proposal for designing of a directly modulated, high Power LASER source capable of operating at 1550 nm wavelength with 40 W Peak Power having pulse width 5 ns and pulse repetition rate >2.3 Mbps. The project also encompasses designing a suitable FSO link in order to understand the nuances in establishing reliable optical communication and subsequent quantification of various atmospheric effects affecting the performance of the FSO link at varying ranges. It also includes extrapolation of such atmospheric effects expected at a link range of 1 Km.

Channel effects on the link have been characterised at different link ranges over a 24 hour cycle, respectively. It was established that Atmospheric Extinction effects like attenuation and scattering are fairly deterministic in nature, while effects due to atmospheric turbulence such as scintillation and beam wander are random in nature owing to instantaneous atmospheric conditions prevalent based upon geographic location of link, temperature,



windspeed affecting channel as well as time of day. These effects need to be quantified statistically.

Attenuation due to Atmospheric extinction based on experimental quantification and extrapolation for a Link range of 1 Km is expected to be 39 dB/Km at day time and 34 dB/Km during the night. It was noted that FSO systems based on coherent light sources such as LASER are plagued with Scintillations and Beam Wander as a result of atmospheric turbulence which are primarily random in nature

Quantification of effects of Atmospheric Turbulence was carried at over a link range of 100 m and corresponding results were extrapolated to link range of 1 Km. It was established that Rytov variance,  $\sigma_R^2$  at 100 m FSO Link varies between 0.5-0.85 over 24 Hour cycle. However, this variance, when extrapolated to a link range of 1000 m is of the order of  $\sigma_R^2 = 10^{-55}$ . Index of Refractive Turbulence  $C_n^2$  is quantified to be of the order of  $10^{-13} \text{ m}^{-2/3}$ . These values are fairly high to qualify for strong fluctuations observed by the receiver at such link ranges. In order to mitigate the effects of such strong turbulence measures, use of Non Imaging Optical systems at the receiver has been recommended based on statistical predictions as established in the Project Thesis.

# TABLE OF CONTENTS

<b>ACKNOWLEDGEMENTS</b>	<b>i</b>
<b>ABSTRACT</b>	<b>ii</b>
<b>LIST OF TABLES</b>	<b>viii</b>
<b>LIST OF FIGURES</b>	<b>ix</b>
<b>ABBREVIATIONS</b>	<b>xi</b>
<b>NOTATION</b>	<b>xii</b>
<b>1. INTRODUCTION</b>	<b>1</b>
1.1 Free Space Optical Communication - An Overview	1
1.2 Applying FSO to Military Specific Scenario	2
1.3 Concept	3
1.4 Challenges	4
1.5 Scope of Project	4
1.6 Project Outline	5
<b>2. OPTICAL TRANSMITTER</b>	<b>7</b>
2.1 Overview	7
2.2 Optical Sources	8
2.2.1 Light Emitting Diode (LED)	8
2.2.2 LASER	8
2.3 Choice of Transmit Wavelength	9
2.4 Designing a Directly Modulated High Power Laser Source	11
2.5 Design Schematic	12
2.5.1 Laser Seed Driver Assembly for Direct Modulation	12

2.5.2	1550 nm CW Laser Seed	12
2.5.3	Master Oscillator Power Amplification	14
2.6	Stages of design for High Power Amplification	15
2.6.1	Pre-Amplification Stage	15
2.6.2	Amplification Stage	17
2.7	Power Budget	18
<b>3.</b>	<b>FREE SPACE OPTICAL LINK BUDGET</b>	<b>21</b>
3.1	Analyzing Link Budget based for Channel without Atmospheric Disturbance	21
<b>4.</b>	<b>MODELLING FSO CHANNEL EFFECTS</b>	<b>25</b>
4.1	Extending Link Budget based for Channel with Atmospheric Disturbance	25
4.2	Diffraction	26
4.3	Atmospheric Extinction Effects	26
4.3.1	Kruse Relation Model for quantifying Atmospheric extinction effects	27
4.3.2	Kim Relation Model for quantifying Atmospheric extinction effects	29
4.4	Influence of Atmospheric Turbulence	30
4.4.1	Physical Effects of Optical Beam Propagation through Random Media	31
<b>5.</b>	<b>EXPERIMENTAL QUANTIFICATION OF CHANNEL EFFECTS USING 532 nm LASER SOURCE</b>	<b>32</b>
5.1	Determining Exact Wavelength of the emitting Laser	32
5.2	Determining Beam Profile of the emitting Laser	33
5.3	Beam Divergence Profile - 531.8 nm Laser Source	34
5.4	Determining Divergence Angle ' $\theta_B$ ' of the Laser Beam	34
5.5	Optical Receiver for FSO Link	35

5.6	Optical Transmitter for FSO Link	37
5.7	Link Bandwidth	37
5.8	Establishing FSO Link - Link Range 100 m	38
5.9	Characterising Traversing angle along Central Axis	39
5.10	Power collected at the Receiver due to Background Radiation (Sun)	40
5.11	Atmospheric Extinction Effects	40
5.11.1	Expected Atmospheric Extinction Effects - Extrapolated to Link range 1000 m	41
5.11.2	Attenuation and Scattering Characterisation - Moderate Fog conditions, Visibility 350 m	42
5.11.3	Expected Atmospheric Extinction Effects, Fog - Extrapolated to Link range 1000 m	42
5.12	Atmospheric Turbulence	43
5.12.1	Kolmogorov Theory of Turbulence	43
5.12.2	Refractive Index Fluctuations	44
5.12.3	Weak and Strong fluctuation conditions	44
5.13	Quantifying effect of Atmospheric Turbulence	45
5.14	Observations and Analysis – Quantification of Atmospheric Turbulence	46
5.14.1	Correlation between Temperature and Humidity	46
5.14.2	Correlation between Temperature and Windspeed	47
5.14.3	Correlation between Variance and Temperature, Windspeed	47
5.14.4	Correlation between Mean and Temperature, Windspeed	48
5.14.5	Correlation between Mean and Variance	49
5.14.6	Refractive Index structure parameter computed based on corresponding Variance	49

5.14.7	Comparative Effect of Atmospheric Optical Turbulence in terms of Variance at a link Range of 1 Km distance	50
5.15	Quantifying Angle of Arrival Fluctuations – FSO Link Range 100 m	51
5.16	Quantifying Beam Wander – FSO Link Range 100 m	52
5.16.1	Analyzing Effect of Beam wander at extended Link Range of 1 Km	55
5.16.2	Experimental quantification of Beam wander at Link Range 60 m	56
5.17	Estimating Probability of Fade	57
5.18	Non Imaging Optics	58
<b>6.</b>	<b>SUMMMARY AND CONCLUSION</b>	<b>60</b>
<b>7.</b>	<b>FUTURE SCOPE</b>	<b>63</b>
7.1	Employing Spatial Diversity Schemes to FSO Link	63
7.2	MIMO-OFDM based FSO system	63
7.3	Exploiting advantages of both RF and FSO Link for establishing communication	63
	<b>REFERNCES</b>	<b>65</b>
<b>A</b>	<b>BILL OF MATERIALS</b>	
<b>B</b>	<b>QUANTIFICATION OF ATMOSPHERIC EXTINCTION EFFECTS</b>	
<b>C</b>	<b>EXPERIMENTAL QUANTIFICATION AND ANALYSIS OF ATMOSPHERIC TURBULENCE BASED ON HISTOGRAM PLOT OVER 24 HOUR CYCLE</b>	

## LIST OF TABLES

Table No	Table Title	Page No
2.1	Atmospheric Optical Transmission Windows	10
2.2	Salient features of the High Speed Laser Driver	12
2.3	Salient features of the High Power Laser Seed	12
5.1	Experimental Quantification of Half Angle of Beam Divergence ( $\theta/2$ )	34

## LIST OF FIGURES

<b>Fig No</b>	<b>Figure Title</b>	<b>Page No</b>
1.1	Bandwidth Capability of RF and Optical Communication Systems	1
1.2	Typical Defence Tactical Scenario	3
1.3	Intensity Modulated Direct Detection FSO System Schematic	4
2.1	Optical Transmitter Block Diagram	7
2.2	PN Junction LED	8
2.3	Concept of LASER	9
2.4	Atmospheric transmittance based on absorption analysis using LOWTRAN	10
2.5	Expected Output of High Power Laser Source	11
2.6	High Power Laser Source Design Schematic	12
2.7	Butterfly packaging of LASER diode	13
2.8	Pre-Amplifier Stage	15
2.9	Energy Level Diagram of Erbium Ions in silica fibers	16
2.10	Amplifier Stage	17
3.1	Beam Divergence	21
3.2	Bit Error Rate Vs Q-Factor	23
3.3	TIA Configuration of Receiver - Direct Detection Method	23
4.1	Various Channels effects affecting performance of FSO Link	25
4.2	Far Field Divergence Angle	26
4.3	Scattering Effects	27
4.4	Simulation Results based on Kruse Model of Atmospheric Extinctions	28
4.5	Simulation Results based on Kim Model of Atmospheric Extinctions	29
4.6	Effect of Atmospheric Turbulence	30
4.7	Laser beam propagation through turbulent atmosphere	31
5.1	Optical wavelength Measurement using LightMtrX	32
5.2	Beam Profile for a collimated Beam - 531.8 nm	33
5.3	Beam Profile for a divergent Beam - 531.8 nm	33
5.4	Narrow Beam Divergence – Laser Source	34
5.5	Beam Divergence Angle	35
5.6	Direct Detection System Schematic	35
5.7	Simulation and Analysis of Integration of Spotter scope with Photo-detector	36

5.8	Integration of Spotter scope with Photo-detector	37
5.9	Circuit Diagram-Driver for LASER for direct Modulation	37
5.10	Link Bandwidth	38
5.11	FSO Link Setup - Transmitter End	38
5.12	FSO Link Setup - Receiver End	39
5.13	FSO Link Setup - 100 m	39
5.14	Freedom of Alignment along Traversing Angle	40
5.15	Experimental Quantification of Atmospheric Extinction (Link Range 250 m)	41
5.16	Analysis and extrapolation of Atmospheric Extinction (Link Range 1000 m)	41
5.17	Experimental Quantification of Atmospheric Extinction – Moderate Fog conditions, Visibility – 350 m (Link Range 100 m)	42
5.18	Analysis and extrapolation of Atmospheric Extinction - Moderate Fog conditions, Visibility – 350 m (Link Range 1000 m)	43
5.19	Typical Turbulent Distorted Data Plot observed at receiver depicting effect of Atmospheric Turbulence on transmitted data	45
5.20	Typical Histogram plot based on data collected	46
5.21	Gaussian Fit on Histogram	46
5.22	Correlation between Temperature and Humidity	46
5.23	Correlation between Temperature and Windspeed	47
5.24	Effect of Temperature and Windspeed on Variance	48
5.25	Effect of Temperature and Windspeed on Mean	48
5.26	Correlation between Mean and Variance	49
5.27	Refractive Index Structure Parameter	50
5.28	Rytov Variance expected at 1 Km FSO Link Range	50
5.29	Angle of Arrival and Image Jitter	51
5.30	Beam Wander	53
5.31	Variance due to Beam Wander- FSO Link 60 m	56
5.32	Fluctuating signal generated at the Receiver	57
5.33	Probability of Fade as a Function of Fade Parameter	58
5.34	Comparison of Imaging and Non Imaging Optical System	59



## **ABBREVIATIONS**

<b>FSO</b>	Free Space Optics
<b>ISR</b>	Intelligence, Surveillance and Reconnaissance
<b>C4ISR</b>	Command, Control, Communication. Computers, ISR
<b>RF</b>	Radio Frequency
<b>LED</b>	Light Emitting Diode
<b>LASER</b>	Light Amplification by Stimulated Emission of Radiation
<b>IR</b>	Infra Red
<b>LNA</b>	Low Noise Amplifier
<b>BER</b>	Bit Error Rate
<b>LOS</b>	Line of Sight
<b>QoS</b>	Quality of Service
<b>MPE</b>	Maximum Permissible Exposure
<b>AEL</b>	Accessible Emission limit
<b>DFB</b>	Distributed Feedback (Laser)
<b>MOPA</b>	Master Oscillator Power Amplifier
<b>MOFA</b>	Master Oscillator Fiber Amplifier
<b>EDF</b>	Erbium Doped Fiber
<b>GBW</b>	Gain Bandwidth Product
<b>IRT</b>	Index of Refraction Turbulence
<b>CW</b>	Continuous wave
<b>dB</b>	Decibels
<b>DSO</b>	Digital Storage Oscilloscope
<b>MIMO</b>	Multiple Input Multiple Output
<b>OFDM</b>	Orthogonal Frequency Division Multiplexing

## NOTATION

$P_{\text{peak}}$	Peak Power
$P_{\text{avg}}$	Average Power
$\tau_l$	Pulse Width
$P_{\text{pump}}$	Pump Power
$P_{\text{in}}$	Input Power
$P_{\text{out}}$	Output Power
$G$	Gain
$\lambda_p$	Pump Wavelength
$\lambda_s$	Source Wavelength
$P_{\text{Tx}}$	Transmit Power
$P_{\text{Rx}}$	Received Power
$G_{\text{Tx}}$	Transmit Antenna Gain
$G_{\text{Rx}}$	Receive Antenna / Telescope Gain
$G_r$	Range Loss
$A_{\text{system}}$	System Dependent Losses
$S_r$	Receiver Sensitivity
$R_\lambda$	Responsivity at wavelength ' $\lambda$ '
$\eta$	Quantum Efficiency
$\sigma_T$	Variance in Thermal Regime
$\sigma_R$	Rytov Variance
$W_B$	Beam Waist
$C_n^2$	Refractive Index Structure Parameter

# CHAPTER 1

## INTRODUCTION

### 1.1 Free Space Optical Communication – An Overview

In the current state of Communication technology, bandwidth hunger seems to be the most dominant aspect among others. The rapid development of the ‘over IP’ services, and the exponential growth of data rates demand dictate the scene, and make it inevitable for Communication System Engineers to address the issue, and explore new frontiers.

In the recent years, attention has been sought to explore a new domain that could participate in the ever increasing pace of today’s communication world, namely Free Space Optics (FSO). FSO refers to a line of sight digital communication technology incorporating broadband data transmission through the atmosphere by means of modulated optical beams.

The primary objective of any long / short haul communication system is to transmit information by modulating this information onto a carrier. Optical frequencies provide a substantial increase (as compared to RF Communication) in the information carrying ability (Bandwidth) that can be received for a given transmitted power.

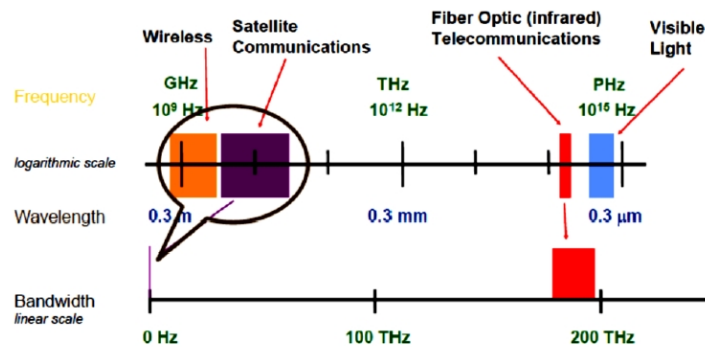


Figure 1.1: Bandwidth Capability of RF and Optical Communication Systems [1]

There are countless applications where FSO technology can prove to be handy, such as last mile connectivity, disaster recovery, metropolitan area networks, backup redundant data links, indoor solution for short range applications, and the Local Area Network (LAN) extension problem, to name a few.

Most prominent attributes of FSO are as under mentioned:

- (a) High speed ratings

- (b) Reliability
- (c) Relatively good coverage for short and medium range applications
- (d) Relative compactness in overall system structure
- (e) Narrow beam divergence
- (f) Ease of deployment
- (g) Inherently high security
- (h) High Megabit per Rupee figure of Merit
- (i) Protocol independence
- (j) License free requirements

## **1.2 Applying FSO to Military Specific Scenario**

In the Defence Environment, operations demand secure, relevant and timely information. The ability to relay massive amounts of information is becoming a critical determinant of military success. For this reason, information superiority on the battlefield is one of the prime objectives. Furthermore, the complexity of military missions has also dramatically increased, with more diverse theatres of operation, expanded spectrums of conflict, and a tremendous increase in the requirement for information to be delivered almost immediately to the war fighter.

With the bandwidth available to FSO anywhere from 100 to 100,000 times higher than other radio frequency or microwave transmitters, use of FSO technology could give the military a much greater leverage over its enemy counterparts. Intelligence, Surveillance, and Reconnaissance (ISR) platforms are seen as a major target for FSO technology as these platforms need to disseminate large volumes of sensor, imagery and video to the fighting forces, often in real-time. Secure wireless backhaul solutions providing a critical component for Command, Control, Communication, Computers, Intelligence, Surveillance and Reconnaissance (C4ISR) is a need of the Hour for today's digitized Battlefield.

In the theatre of operation, deployment of a wireless network / link needs to happen in hours. Fast installation and trouble free operation even in the harshest cold and extreme hot weather conditions is of paramount importance. Whether the need is to monitor the perimeter of a base/camp, provide broadband access for personnel or deploy in disaster management role, FSO communication systems exhibit the capability of installation at short notice in an

extremely cost effective manner. These solutions exhibit a unique capability of not being intercepted and detected by wireless RF eavesdropping.

FSO Communication Systems have the ability to provide both permanently installed broadband communications solutions and temporary/emergency platforms for tactical and intelligence applications. For military base installations, where buildings often encompass a large geographic region, fixed broadband radios and laser links can provide a cost effective, simple and secure solution when compared to the cost of wired coax and fiber alternatives.

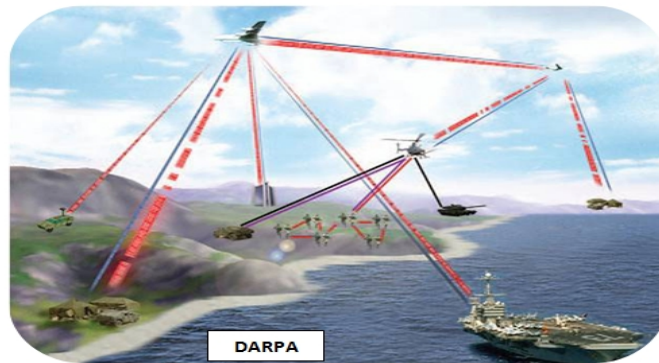


Figure 1.2: Typical Defence Tactical Scenario

### 1.3 **Concept**

A typical FSO system consists of an optical transmitter, an optical receiver, and an interfacing device which mediates between the data source and the optical transceivers. An optical transmitter consists of a driving circuit that feeds a Light Emitting Diode (LED) / LASER with an electrical modulating signal, which in turn is converted by the optical source into a modulated optical beam, namely an Infra Red (IR) / visible beam, which is further collimated by a lens before being transmitted through the atmosphere.

At the receiving end, the optical beam is focused by a receiving lens on a high sensitivity P-I-N photo-detector. The photo-detector converts a certain level of power intensity into a corresponding level of electrical current. The photo-detector is connected to a Low Noise Amplifier (LNA) for achieving better Bit Error Rate (BER) performance. The LNA in turn converts the photo-current to an appropriate voltage level before passing it to subsequent amplification stages, needed for proper data retrieval.

FSO requires a clear Line Of Sight (LOS) between the transmitter and the receiver for the collimated optical beam to propagate through the atmosphere without being intercepted. A

proper alignment practice is required as well. Misalignment would result in a complete dropout or degradation of the link in terms of the effective link range.

FSO communication can be established in Full Duplex Mode by incorporating Transmitter - Receiver pair in one FSO Link, suitably operating in two specifically different wavelengths for optical data transmission.

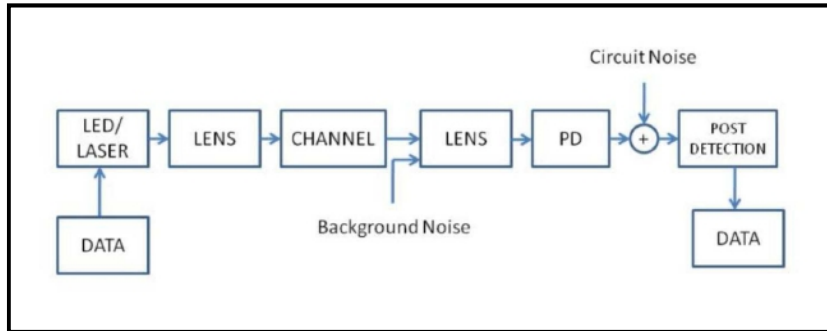


Figure 1.3: Intensity Modulated Direct Detection FSO System Schematic

#### 1.4 Challenges

The fundamental challenges of FSO communications are imposed by atmospheric phenomena, which tend to attenuate the optical power in the transmitted beam, hence decreasing the effective link distance. Such phenomena, which affect the overall link performance, are absorption and scattering which are a result of atmospheric molecules, aerosols as well as black carbon molecules having molecular size equivalent to the order of wavelength transmitted. Although insignificantly affected by rain and snow, FSO communication systems ‘Quality of Service (QoS)’ can be extremely degraded by fog and atmospheric turbulence leading to effects like Beam Wander and scintillation which are majorly stochastic and time varying in nature and turn out to be a major obstacle in developing accurate channel models with reference to a particular geographical location. These phenomena, however, should be accounted for while designing an efficient FSO system.

#### 1.5 Scope of Project

- (a) Identify suitable components and propose a detailed design for a High Power, 1550 nm LASER Source capable of operating at 40 W Peak Power, 5 ns Pulse width having data rate > 2.3 Mbps.

- (b) Setup a Free Space Optical Communication Link with a suitable transmitter / receiver design for a link range of 250 m.
- (c) Carry out detailed performance analysis of the FSO Link under varying atmospheric conditions over a 24 hour cycle and quantify various channel effects affecting the link performance at a predefined range.
- (d) Extrapolate and analyze the channel effects for link range of 1 Km. Verify the experimental results with existing theoretical models and draw appropriate conclusions.

## **1.6 Project Outline**

Project Thesis has been compiled in 7 Chapters for ease of understanding and putting forth a factual correlation of theory researched and experiments conducted towards the completion of the project.

**Chapter 2** Brings out the fundamentals involved in developing an Optical Transmitter for Free Space Communication. It discusses in detail the design for developing a high power Laser source as the first requirement of the project. It also works out the Power Budget of the Laser Source designed.

**Chapter 3** This chapter theoretically analyzes the Free Space Optical Link Budget based on channel without Atmospheric disturbance with relevance to the high power Laser source designed and Receiver sensitivity. It allows us to understand the link margin available with the FSO Link at specific Link ranges.

**Chapter 4** Builds up theoretical understanding about channel effects affecting FSO Link performance and brings out simulation studies on existing channel models in order to quantify Atmospheric extinction effects.

**Chapter 5** Brings out in detail FSO Link setup at 100 m / 250 m and all experiments undertaken with a 531.8 nm Laser Source to quantify channel effects affecting FSO link performance. This chapter also builds up an understanding for quantifying effects of Beam Wander and Scintillation arising out of Atmospheric Turbulence. All channel effects have been suitably quantified for varying link ranges over a 24 Hour cycle and their corresponding effect on FSO link has been suitably extrapolated and analysed for link range of 1000 m.

**Chapter 6** In this chapter, we bring about the conclusion of project work and summarize key results and observations.

**Chapter 7** Here we discuss the future projects that could be undertaken in this field of work in order to enhance performance of FSO Link.



## CHAPTER 2

### OPTICAL TRANSMITTER

#### 2.1 Overview

The transmitter aims to produce a suitable signal for transmission. It is the stage between the interfacing circuit on one side, and the channel on the other side. Transmitter takes its input signal from the interfacing circuit, and positions its output onto the channel. Hence, the design of the transmitter largely depends on the output of the interfacing circuit, and the characteristic of the channel.

The transmitter mainly consists of three parts, the first part being a conditioning and driving circuit. The main purpose of this part is to take the data signal from the interfacing circuit and modify it so as to provide the light source with a suitable driving signal to emit the required optical signal. Also, this part should be able to compensate for any undesirable effect or noise that may occur due to factors like optical source temperature variation or any injected noise to the system. The second part consists of a light source that emits an optical signal suitable for transmission. This optical signal is an emitted light for a certain period of time with a certain power to represent high LOGIC level, and emits nothing to represent low LOGIC level. The optical light source could be of two types:

- (a) Light Emitting Diode (LED)
- (b) LASER

The third part comprises of a collimated lens arrangement used to direct the output of the light source precisely in order to attain a good distance between the transmitter and the receiver with very low beam divergence.

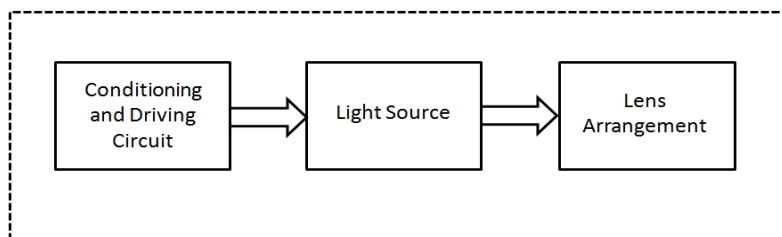


Figure 2.1: Optical Transmitter Block Diagram

## 2.2 Optical Sources

Optical light sources are primarily divided into two broad categories:

### 2.2.1 Light Emitting Diode (LED)

The LED is a semiconductor device and an optical source which radiates an optical beam when a forward bias voltage is applied to it. The mechanism of the LED is based on a p-n junction. Applying direct voltage to the LED terminals makes a flow of electrons from the n-side (anode) to the p-side (cathode). Each electron, by reaching the hole on the p-side releases energy in the form of a photon. The wavelength of the radiated photon depends on the energy gap between semiconductor materials. A basic LED diagram is shown:

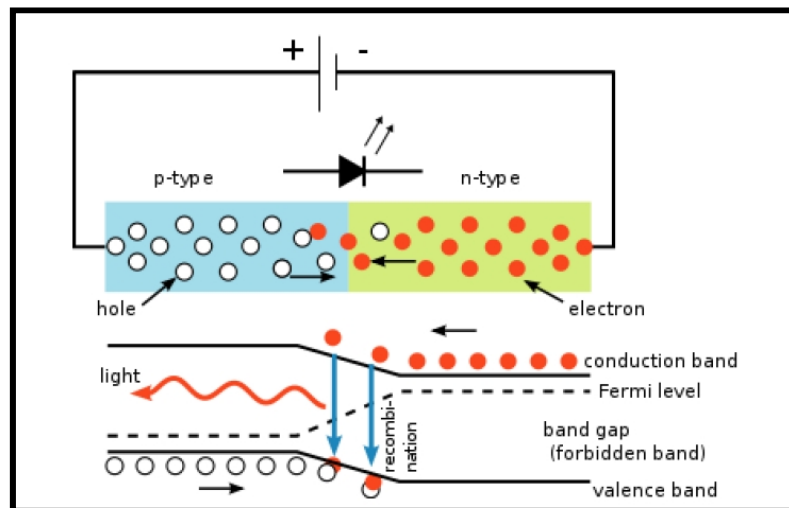


Figure 2.2: PN Junction LED

LEDs are low cost devices. These belong to the class of low power devices. As LEDs exhibit high beam divergence and non-coherent beam characteristics, they are considered to be eye safe light sources.

### 2.2.2 LASER

LASER is the acronym for Light Amplification by Stimulated Emission of Radiation [2]. Stimulated emission is a process in which the incident photon causes the excited electron to go to a lower energy level and during this transition radiates a photon with same phase and frequency of the incident photon.

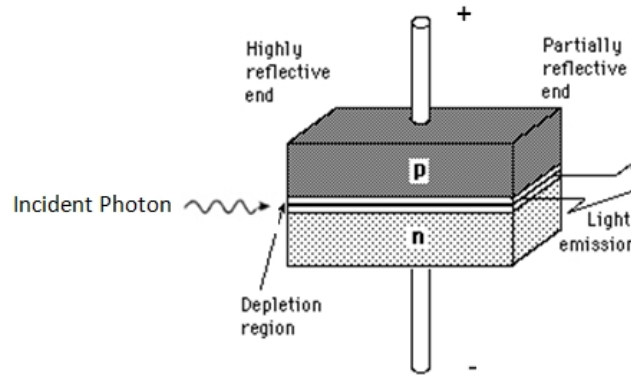


Figure 2.3: Concept of LASER

In order to produce a coherent beam of photons, direct bias voltage is applied to the diode. This causes the flow of electrons towards the p-type region and holes into the n-type region and as a result, an electron-hole pair is generated. In laser applications this is called ***pumping***. In this case, emission of a photon leads to the recombination of electron-hole pairs. The result of this recombination is the production of an additional photon with the same frequency and phase as the first photon.

These photons, the input photon and the generated one, can be guided out of the semiconductor or can also be used to generate more photons. One usual way to reach this goal is by using two mirrors (Fabry Perot arrangement), one perfect mirror which reflects all incident photons and another partial mirror which reflects just a portion of the photons and transmits the rest. Trapped photons can be used to stimulate more electrons and therefore more generation of photons. Those photons which pass through the partial mirror are the laser beam output.

LASERS have the ability to produce a uniform monochromatic beam that is highly directional, having a very low beam divergence. This difference allows lasers to focus light and energy on very small surfaces, even on far-away objects, a unique characteristic that lends itself suitable for larger link range FSO communication systems.

### 2.3 Choice of Transmit wavelength

Choice of Transmit wavelength in FSO essentially depends upon following parameters:

(a) **Ease of availability** (Laser Source wavelength) and compatibility with existing Fiber Optic Technology for effective merger of both, in order to improve overall Network Efficiency. 1550 nm wavelength is extensively used in setting up Fiber Optic links in Telecommunication Industry.

(b) Efficient exploitation of advantages of **Atmospheric Optical Transmission window** [3] (Figure 2.4). It has been well established that certain wavelengths, while being transmitted through atmospheric channel undergo comparatively lower attenuation as compared to the rest. Such wavelengths would be more suitable for establishing FSO Link. Table 2.1 gives an overview of suitable transmit wavelength bands based on extensive evaluation of various atmospheric content databases. 1550 nm wavelength exhibits high Transmittance in Atmospheric channel.

I	II	III	IV	V	VI	VII	VIII
0.30	0.97	1.16	1.40	1.95	3.00	4.5	7.7
0.92	1.10	1.30	1.80	2.40	4.20	5.2	14

Table 2.1: Atmospheric Optical Transmission Windows (Windows Start and Stop wavelength given in  $\mu\text{m}$ )

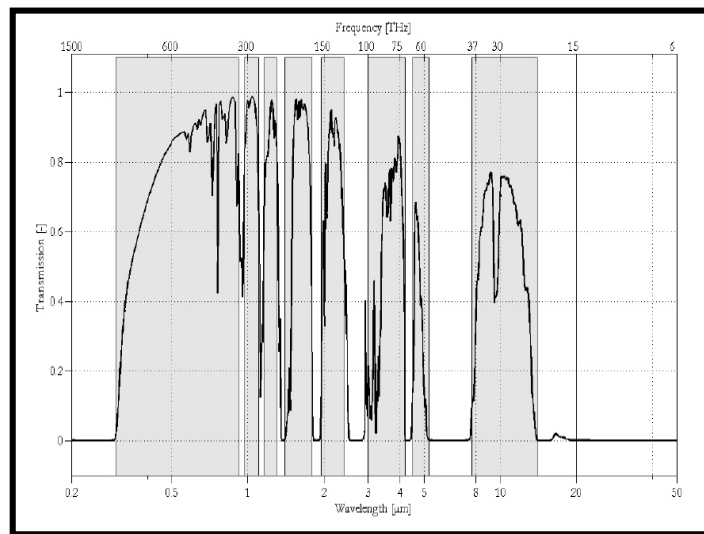


Figure 2.4: Atmospheric transmittance based on absorption analysis using LOWTRAN

(c) **Human safety** is the highest priority in employing any kind of technology. Laser systems which operate between 0.18  $\mu\text{m}$  and 1 mm wavelengths may cause biological damage to the eye and skin. IR and visible lasers are located in this window. Applying them in FSO systems should be followed as per laid down safety considerations.

(d) **Maximum Permissible Exposure (MPE)** is the level of laser radiation that is considered safe for an unprotected human eye. Its unit is either  $\text{W}/\text{cm}^2$  or  $\text{J}/\text{cm}^2$  and is measured at the cornea of the human eye. MPE value depends on the exposure duration of the laser beam to the eye and it decreases as the exposure time increases.

(e) **Accessible Emission Limit (AEL)** is a metric used in laser classifications. It is essentially the corresponding power at which the maximum emission level lies in a particular hazard class and its unit is Watts. Point sources AEL can be found by multiplying the area of limiting aperture by the MPE value.

There are two major laser wavelengths that are used in FSO systems. For a specific amount of exposure time, it has been ascertained that the 1550 nm laser has a much higher MPE than 850 nm. This is due to the fact that most of the beam energy at the 1550 nm wavelength is absorbed by the cornea of the eye before being focused on the retina. This means a higher laser power can be used to transmit data with 1550 nm than with 850 nm without exceeding the safety limits based on internationally recognized Laser safety standards [4]. Hence, it is ascertained that **1550 nm wavelength** is the most preferred wavelength for establishing FSO based communication system.

#### 2.4 Requirement 1 - Designing a Directly Modulated High Power Laser Source

Based on the above understanding, first requirement of the project was to identify suitable components and propose a detailed design for a directly modulated High Power Laser Source having following design parameters.

- (a) Wavelength of source : 1550 nm
- (b) Peak Power : 40 W
- (c) Pulse Width : 5 ns
- (d) Data Rate > 2.3 Mbps

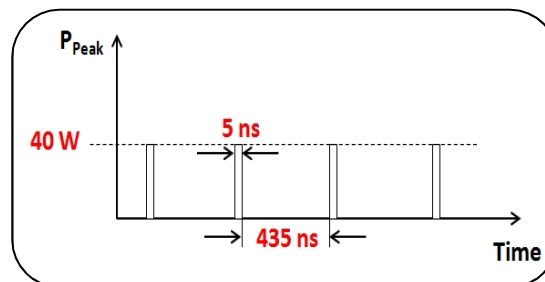


Figure 2.5: Expected Output of High Power Laser Source

## 2.5 Design Schematic

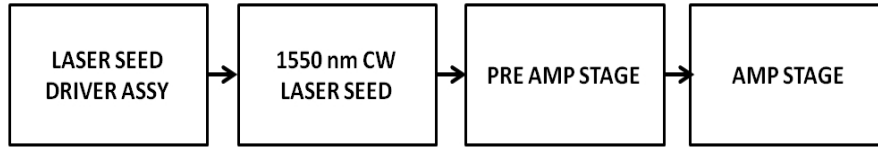


Figure 2.6: High Power Laser Source Design Schematic

### 2.5.1 Laser Seed Driver Assembly for Direct Modulation

Laser seed driver assembly should be capable of giving electrical pulses with a very narrow output pulse width of at least 5 ns. It should have a high pulse repetition rate in order to meet project specific requirements. The Driver assembly should be compatible with commercially available LASER diode package in terms of current rating and pin configuration. Extensive global market survey was carried out and *Picolas (Laser Components) BFS-VRM 03 HP High Speed Laser Driver* was found to be the most suitable for project requirement.

Analog Modulation	DC to 400 MHz
Output Pulse Width	1 ns to CW
Output Current	0-3A Pulse , 0.5 A CW
Repetition Rate	30 MHz
Input Power	+5V DC

Table 2.2: Salient features of the High Speed Laser Driver

### 2.5.2 1550 nm CW Laser Seed

The CW Laser seed proposed after extensive market survey is *Thorlabs 1550 nm FP Laser Diode – Model FPL1009S*. The butterfly packaged Laser seed was found to be compatible with the Laser Driver specifications as proposed above.

Maximum Operating Current	500 mA
Center Wavelength	1550 nm
Output Power (CW)	> 100 mW ~ 20 dBm

Table 2.3: Salient features of High Power Laser Seed

Figure 2.7 shows a typical butterfly-style package in a cross-sectional view. The package consists of metal, typically Kovar. An optical fiber pigtail is attached to one of

the front-end sides. Electrical leads feed through the sidewalls of the package. The electrical traces are embedded in ceramic material for electrical isolation.

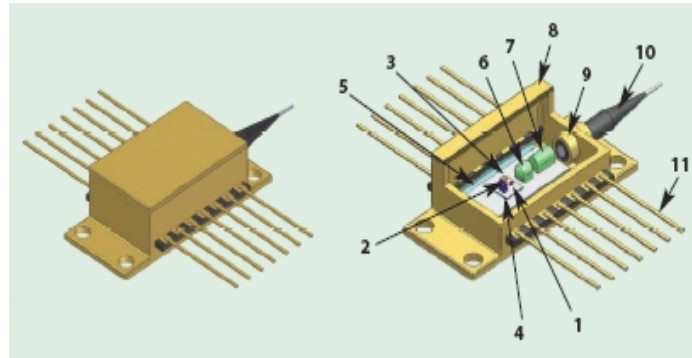


Figure 2.7: Butterfly package for showing laser chip (1), monitor photodiode (2), thermistor (3), chip carrier (4), thermoelectric cooler (5), lens (6), optical isolator (7), component package (8), window for light output (9), fiber pigtail (10) and electrical leads (11)

Inside the transmitter package is the chip carrier with the laser chip mounted on it. A thermistor is mounted on the same carrier to track the temperature of the laser. The thermistor signal is used in the external control circuit as a feedback signal to adjust the power of the thermoelectric cooler (TEC) at the base of the package. The TEC stabilizes the laser temperature, typically within  $\pm 1^\circ\text{C}$  or less. The temperature stability requirement is determined by the specification for the emission wavelength of the transmitter, since the temperature determines the emission wavelength of the laser.

A monitor photodiode is mounted facing the back facet of the laser chip for output power control. The signal from the monitor photodiode is used by the external control circuit to adjust the laser current. The typical requirement for output power stability is less than 0.5 dB over temperature and lifetime. Sometimes the monitor photodiode is placed at the front side. In this case, a portion of the output light beam is tapped off with a semi-transparent mirror and directed onto the monitor photodiode.

The laser emission is collimated by a lens mounted close to the laser facet. The lens is typically an aspheric glass lens with a relatively high numerical aperture to capture most of the light from the laser. Since the laser output beam is quite elliptical with a larger divergence angle in the vertical than in the horizontal direction, the coupling efficiency into the single-mode fiber is limited to about 50 percent. The collimated laser beam travels through an optical isolator before being coupled into the fiber. The optical isolator is necessary for distributed feedback (DFB) lasers. It prevents light of

parasitic reflections from re-entering the laser cavity. Without an isolator, the DFB laser emission can become very noisy and the optical system does not operate well.

### **2.5.3 Master Oscillator Power Amplification**

The term *Master Oscillator Power Amplifier (MOPA)* refers to a configuration consisting of a master laser (or seed laser) and an optical amplifier to boost the output power. A special case is the *Master Oscillator Fiber Amplifier (MOFA)* [5], where the power amplifier is a fiber device, usually a cladding-pumped high-power amplifier, often based on an ytterbium-doped fiber. The main attractions of such fiber based power amplifiers are:

- (a) High output power can be achieved with a high power efficiency.
- (b) The cooling system can be relatively simple.
- (c) The gain can easily be as high as tens of decibels.
- (d) With a MOFA instead of a laser seed, it can be easier to reach the required performance e.g. in terms of linewidth, wavelength tuning range, beam quality or pulse duration if the required power is very high. This is because various performance aspects are decoupled from the generation of high powers. This gives extra flexibility, e.g. when a gain-switched laser diode is used as a seed laser.
- (e) The same aspects apply to other kinds of modulation, e.g. intensity or phase modulation: it may be advantageous to modulate the low-power seed laser, rather than to modulate a high-power device directly.
- (f) The combination of an existing laser with an existing amplifier (or an amplifier chain) may be simpler than developing a new laser with higher output power.

However, the use of fiber also has disadvantages:

- (a) Various kinds of fiber nonlinearities can make it difficult to reach very high peak powers and pulse energies in pulsed systems. In single-frequency systems, stimulated Brillouin scattering (SBS) can severely limit the output power.



(b) Due to the high gain, fiber amplifiers are relatively sensitive to back-reflections, which are amplified again before entering the master laser. This feedback sensitivity can often be cured by placing a Faraday isolator behind the amplifier.

(c) The polarization state is often undefined and unstable, unless polarization-maintaining fibers are used.

It is attractive to use a gain-switched laser diode as seed laser for a fiber MOPA. Such devices compete with Q-switched lasers. Their advantages partly lie in their flexibility concerning output formats. It is easy to modify not only the pulse repetition rate but also the pulse duration and shape, and pulse energy.

A special aspect of MOFAs is that the saturation power, even of a large mode area double-clad fiber is low as compared to the typical output power. Therefore, the power extraction can be as efficient as in a fiber laser, even for relatively low seed powers.

## 2.6 Stages of design for High Power Amplification

### 2.6.1 Pre-Amplification Stage

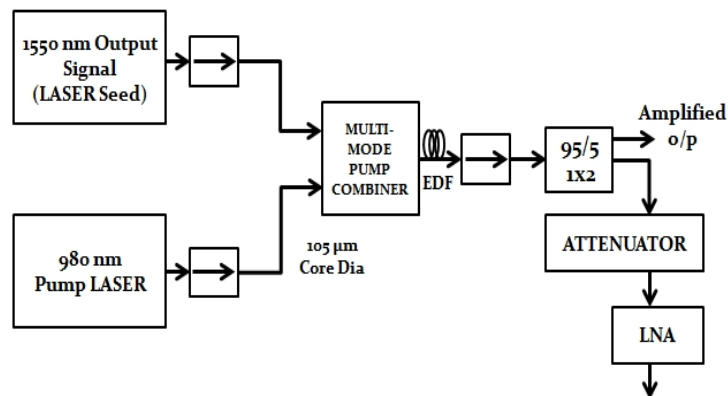


Figure 2.8: Pre-Amplifier Stage

The First Stage of amplification as brought out in Figure 2.8 is the Pre-Amplification stage. Typical Peak output power level expected from the Laser seed is ~80 mW (From Datasheet). This output from the Laser seed along with output from a 980 nm CW Pump Laser is fed as input to the Multimode Pump Combiner (in forward pumping configuration) which allows the powers of these two mutually incoherent

beams to be combined without a power loss. This combined power is made to pass through a Si Fiber doped with  $\text{Er}^{3+}$  (Erbium Ions). The gain spectrum depends on the pumping scheme and presence of dopants like  $\text{Er}^{3+}$  within the fiber core. Erbium doped fibers have the ability to provide high gain to the tune of 30 dB [6] while operating in wavelength region near 1550 nm. Most fiber Amplifiers use 980 nm pump lasers as such lasers are commercially available and can provide more than 100 mW of Pump Power. The amplified output from the Erbium Doped Fiber, EDF is made to pass through 2x1 95/5 Coupler where 95% amplified output is made to pass through an isolator (in order to absorb back reflections, if any) to the (second) Amplification stage cascaded to the Pre-Amplification stage. 5% amplified output is monitored through an LNA at the end of Pre-Amplification stage.

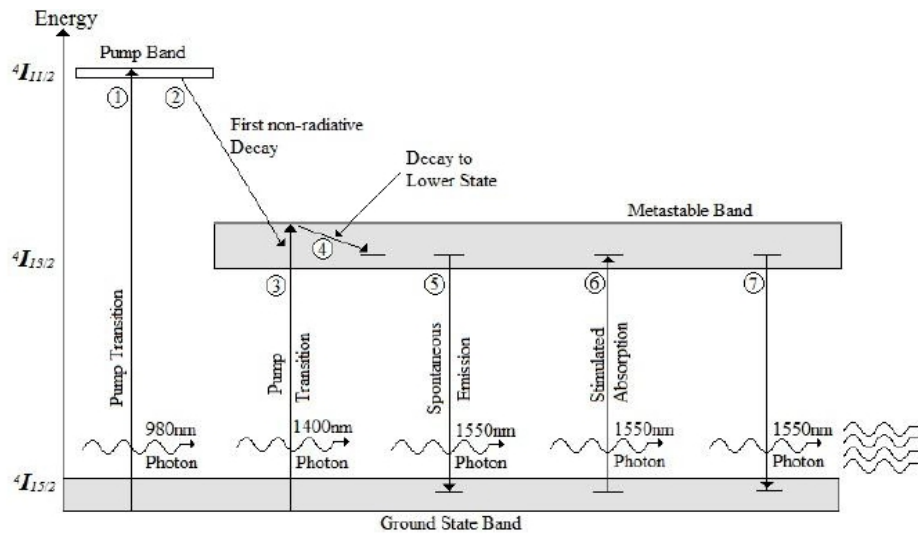


Figure 2.9: Energy Level Diagram of Erbium Ions in silica fibers

The population inversion condition required in the amplifier material is achieved with the help of the power from the pump source. Once the population inversion is created, there are large number of electrons in the metastable state that undergo stimulated emission to jump to the ground state. As power of the input signal increases, these large number of excited electrons undergo stimulated emission and the output optical signal is highly amplified (Figure 2.9). However, as this process continues, the number of excited electrons in the metastable state start decreasing and the population inversion condition starts depleting. As a result, the gain of the EDFA drops due to unavailability of sufficient excited electrons to undergo stimulated emissions. Thus at very low input optical powers, EDFA shows a high gain and as this power increases, there is a decrease in the gain of the device. This observation clearly suggests the

insufficiency of the power supplied by the pump source in creating required population inversion condition in the EDFA. This situation can be mathematically expressed in terms of an equation which is based on the conservation of photons in the entire process of amplification of the input optical signal [16]. The equation is given as:

$$P_{out} \leq P_{in} + \frac{\lambda_p}{\lambda_s} P_{pump}$$

The ratio  $\lambda_p/\lambda_s$  signifies the number of photons supplied by the pump source in the process of amplification of the input signal.

The Pump Laser seed proposed for power amplification is *Gooch and Housego 500 - 700 mW Single Mode Pump Lasers AC1401-0700-0980-SM*.

### 2.6.2 Amplification Stage

The Second Stage of amplification as brought out in Figure 2.10 is the Amplification stage. The general layout of the amplification is similar to the pre-amplification stage except for the fact that this particular stage handles higher power levels than the initial stage. Due to this particular reason, the gain medium is chosen to be *Erbium ytterbium doped double clad fiber* which essentially allows cladding pumping, capable of boosting the output power of 1550 nm laser sources to very high levels.

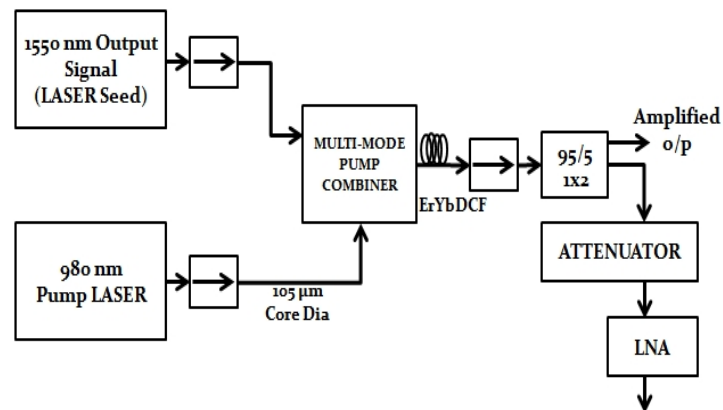


Figure 2.10: Amplifier Stage

In a Double Clad Fiber, the laser light propagates in a single-mode (or multimode) core, which is surrounded by an *inner cladding* in which the pump light propagates. Only the core is rare-earth-doped. The pump light is restricted to the inner cladding by an outer cladding with lower refractive index, and also partly propagates

in the single-mode core, where it can be absorbed by the laser-active ions. The inner cladding has a significantly larger area compared to core and typically a much higher numerical aperture, so that it can support a large number of propagation modes, allowing the efficient launch of high power Laser output [7].

The broad gain bandwidth of Erbium ytterbium doped double clad fiber is suitable for the amplification of ultrashort pulses. However, limitations arise from fiber nonlinearities such as the Kerr effect, which can lead to strong self-phase modulation and Raman effect leading to the generation of a strong first-order Stokes wave at a wavelength, tens of nanometers longer than that of the amplified signal. Single-frequency signals can also be amplified to high powers. In this case, stimulated Brillouin scattering usually sets the limits.

## 2.7 Power Budget

Here we carry out calculation of power budget of the sub system by assuming that the Peak power required at output is  $\approx 80 \text{ W} = 49.03 \text{ dBm}$

In order to achieve 49.03 dBm (80 W) peak power, Average Power Requirement would be calculated as follows

$$P_{\text{peak}} = \text{Energy} / \tau_l \quad (\text{Where, } \tau_l \text{ is desired pulse width, } 5\text{ns})$$

$$\text{Energy} = 80 \times 5 \times 10^{-9} = 4 \times 10^{-7} \text{J}$$

$$P_{\text{avg}} = \text{Energy} \times \text{Repetition Rate}$$

$$= 4 \times 10^{-7} \times 2.3 \times 10^6 = 0.92 \text{W} = \mathbf{29.637 \text{ dBm}} \quad (\text{Data Rate} = 2.3 \text{ Mbps})$$

Alternatively,

$$\text{Time Period} = 1 / \text{Data Rate} = 1 / 2.3 \times 10^6 = 4.3478 \times 10^{-7} \text{ sec}$$

$$\text{Duty cycle} = \text{Pulse Width} / \text{Time Period} = 5 \times 10^{-9} / 4.3478 \times 10^{-7} = 0.0115 = \mathbf{1.15\%}$$

$$P_{\text{Avg}} = P_{\text{Peak}} \times \text{Duty Cycle} = 80 \times 0.0115 = \mathbf{0.92 \text{ W} = 29.637 \text{ dBm}}$$

**Minimum output  $P_{\text{peak}}$  expected from Laser Seed  $\approx 80 \text{ mW} = 19.03 \text{ dBm}$  (From Datasheet)**

In order to achieve desired Average Power at output, we require two stages of amplification.

### Pre-amplifier Stage - EDFA comprising of Single Clad Erbium doped fiber

At Pre-amplifier Stage,

Peak Power,  $P_{in} = 80 \text{ mW}$

Average Power,  $P_{in (avg)} = 0.92 \text{ mW} = -0.36 \text{ dBm}$

We know,

$$P_{in (avg)} \times (G-1) < P_{pump}$$

$$0.92 \times (G-1) < 700$$

Hence,  $G < 761.869 \sim 28.818 \text{ dB}$  (Max Gain Possible)

Also,

$$\begin{aligned} P_{out} &= P_{in} + (\lambda_p/\lambda_s) \times P_{pump} \quad [16] \\ &= 0.92 + (980/1550) \times 700 = \mathbf{443.5 \text{ mW}} \end{aligned}$$

Typical achievable gain from Preamplifier stage  $\sim 26.83 \text{ dB}$

Min expected Gain = 20 dB

Hence, after 1<sup>st</sup> Stage of Amplification,  $P_{out (Avg)} = 19.64 \text{ dBm} = \mathbf{84.68 \text{ mW}}$

**Peak Power on First Stage Amplification = 7.363 W**

### Amplifier Stage - EDFA comprising of Double Clad Erbium Ytterbium doped fiber

At Amplifier Stage,

$$P_{in} = 84.68 \text{ mW} = 19.64 \text{ dBm}$$

We know,

$$P_{in} \times (G-1) < P_{pump}$$

$$84.68 \times (G-1) < 700$$

Hence,  $G < 9.266 \sim 9.67 \text{ dB}$  (Max Gain Possible)

Also,

$$\begin{aligned} P_{out} &= P_{in} + (\lambda_p/\lambda_s) \times P_{pump} \\ &= 84.68 + (980/1550) \times 700 = \mathbf{527.26 \text{ mW}} \end{aligned}$$

Typical achievable gain from Amplifier stage  $\sim 7.94 \text{ dB}$

Hence, after 2<sup>nd</sup> Stage of Amplification,  $P_{out} = 27.58 \text{ dBm} \sim \mathbf{572.796 \text{ mW}}$

**Minimum Peak Power on Second Stage Amplification = 49.8008 W**

**Peak Power (Expected) =  $P_{\text{Avg}} / \text{Duty Cycle} = 0.572796 / 0.0115 = 49.808 \text{ W} \approx 46.97 \text{ dBm}$**

Bill of Material requirement for the Project is discussed in detail in **Appx 'A'** to the Thesis Report.

## CHAPTER 3

### FREE SPACE OPTICAL LINK BUDGET

#### Modulation Scheme Proposed: On-Off Keying

Link Budget is analyzed in two stages based on above mentioned components.

#### 3.1 Analyzing Link Budget based for Channel without Atmospheric Disturbance

In the basic free-space channel the optical field generated at the transmitter propagates only with an associated beam spreading loss. For this system, the performance can be determined directly from the power flow. The signal power received  $P_{Rx}$  [W] depends on the transmit power  $P_{Tx}$  [W], transmit antenna gain  $G_{Tx}$ , receive antenna gain  $G_{Rx}$ , the range loss  $G_r$  and system-dependent losses  $A_{system}$  [3]

$$P_{Rx} = P_{Tx} \cdot G_{Tx} \cdot G_r \cdot G_{Rx} \cdot A_{system}$$

Assuming, we are able to achieve desired gain from EDFA, we expect a  $P_{Tx} = 40 \text{ W}$  (Calculations based on high power laser source designed in chapter 2 of the Thesis).

Assuming a Gaussian beam under filling the transmit aperture (The collimator Lens proposed for the project is capable of emitting light in a Gaussian Beam Profile), the *transmit antenna gain*,

$$G_{Tx} = 32/\theta^2$$

Where,  $\theta$  [rad] is the full-angle  $e^{-2}$  divergence of the transmit beam.

$$1^\circ \approx 17.45 \text{ mrad} \rightarrow 1 \text{ mrad} \approx 0.0573^\circ$$

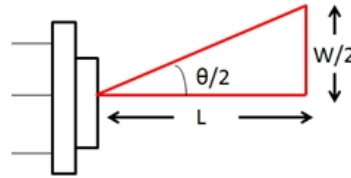


Figure 3.1: Beam Divergence

It was experimentally found that Beam Divergence Angle,  $\theta = 0.194^\circ$

$$\theta = 0.194^\circ = 3.3853 \text{ mrad}$$

Therefore,  $G_{Tx} = 32/(3.3853 \times 10^{-3})^2$

$$G_{Tx} = 2.79 \times 10^6$$

The **Range loss**,  $G_r$  depends on the link propagation distance 'L' and is given by:

$$G_r = \left( \frac{\lambda}{4\pi L} \right)^2$$

Quantifying propagation effect on Link Distance = 1 Km,

$$G_r = (1550 \times 10^{-9} / 4\pi \cdot 1000)^2$$

$$G_r = 1.5214 \times 10^{-20}$$

The **receive antenna gain**, with telescope aperture diameter (antenna size) 'D', is given by:

$$G_{Rx} = \left( \frac{\pi D}{\lambda} \right)^2$$

Effective Diameter of Telescope Aperture, D = 50 mm

$$\text{Therefore, } G_{Rx} = (\pi \times 50 \times 10^{-3} / (1550 \times 10^{-9}))^2$$

$$G_{Rx} = 1.027 \times 10^{10}$$

$A_{system}$  reflects all the other system-dependent losses. It includes losses due to link misalignment, pointing Losses, telescope losses, etc.

$$\text{Assuming, } A_{system} \text{ (dB)} = -6 \text{ dB} = 0.2511886$$

Hence,

$$P_{Rx} = P_{Tx} \cdot G_{Tx} \cdot G_r \cdot G_{Rx} \cdot A_{system}$$

$$P_{Rx} = 40 \times 2.79 \times 10^6 \times 1.5214 \times 10^{-20} \times 1.027 \times 10^{10} \times 0.2511886$$

$$= 0.00438 \text{ W} = 6.419 \text{ dBm}$$

$$\text{Therefore, } P_{Rx} = 4.38 \text{ mW} = 6.419 \text{ dBm}$$

Because of the absence of atmospheric effects the Link Margin  $M_{link}$  in dB is given by:

$$M_{link} \text{ [dB]} = P_{Rx, dBm} - S_r$$

Where,  $S_r$  is the Receiver Sensitivity (Direct Detection Method)

Estimating Receiver Sensitivity,  $S_r$

Assuming, minimum acceptable Bit Error Rate (BER) =  $10^{-12}$



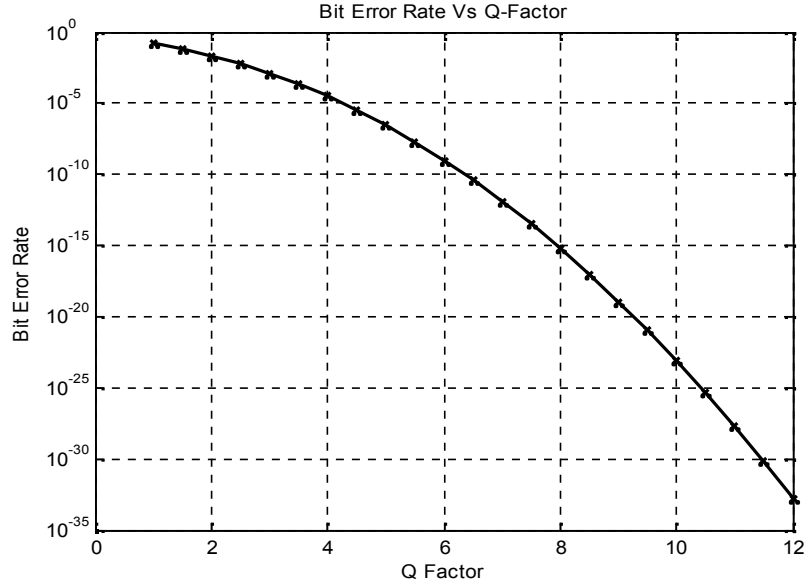


Figure 3.2: Bit Error Rate Vs Q-Factor [6]

From Figure 3.2, for  $BER = 10^{-12}$ , corresponding Q-Factor = 7 (Minimum BER expected)

Also,

Wavelength,  $\lambda = 1550$  nm

Bit rate  $\approx 2.3$  Mbps

Noise Bandwidth of LNA,  $\Delta f = 25$  MHz (Based on TIA Configuration)

OpAmp used for designing LNA is OPA 656,

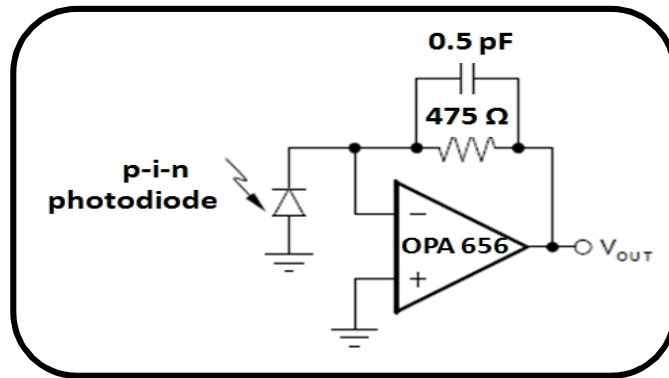


Figure 3.3: TIA Configuration of Receiver – Direct Detection Method

$$\Delta f = \sqrt{\frac{GBW}{2\pi R_L C_f}}$$

Where, Gain Bandwidth Product,  $GBW = 10^6$

Hence, Noise Bandwidth,  $\Delta f = 25.886$  MHz  $\approx 25$  MHz

Here, we propose to use InGaAs, p-i-n Photodetector, having 65 % quantum Efficiency,

$$\eta \approx 0.65$$

Load Resistance,  $R_L = 475 \Omega$

We Know,

$$\text{Responsivity, } R_\lambda = \frac{\eta \lambda (\mu m)}{1.24} = \mathbf{0.8125 \text{ A/W}}$$

Also,

$$\sigma_T^2 = \left[ \frac{4k_B T}{R_L} \right] f_n \Delta F = 8.722 \times 10^{-16}$$

Where,  $T = 300 \text{ K}$

Boltzmann Constant,  $k_B = 1.381 \times 10^{-23}$

Noise Figure,  $f_n = 1$

Hence,

$$\sigma_T = \mathbf{2.9533 \times 10^{-8}}$$

Now,

$$\text{Receiver Sensitivity, } S_r = \frac{Q}{R_\lambda} (qQ\Delta F + \sigma_T) = 0.255 \mu\text{W} \approx \mathbf{-35.94 \text{ dBm}}$$

Here,

Electron Charge,  $q = 1.6 \times 10^{-19} \text{ C}$

Hence overall Link Margin  $M_{\text{link}}$  in dB,

$$\begin{aligned} \mathbf{M_{link} [dB]} &= \mathbf{P_{Rx,dBm} - S_r} \\ &= 6.419 - (-35.94) \\ &= \mathbf{42.359 \text{ dB}} \end{aligned}$$

This high Link Margin is very important in order to suitably cater for heavy losses arising in the atmospheric channel due to presence of Aerosols, black carbon particles and random effect Atmospheric Turbulence, thereby affecting overall performance of FSO Link at higher link ranges. The same are discussed in chapter 4.

## CHAPTER 4

### MODELLING FSO CHANNEL EFFECTS

#### 4.1 Extending Link Budget based for Channel with Atmospheric Disturbance

All systems utilizing optical waves must take into account general propagation effects associated with the medium in which it propagates in addition to the effects associated with the wave itself. A number of fundamental phenomena concerning optical wave propagation in a random medium are important for analysis. These are *Diffraction, Atmospheric Extinction and Atmospheric Turbulence*.

In order to consider the effects disturbing a link propagating through the Earth's atmosphere the link equation discussed in chapter 3 needs to be extended. The three primary atmospheric phenomena that affect optical wave propagation are *absorption, scattering and refractive index fluctuations* (i.e., optical turbulence). Absorption and scattering by the constituent gases, aerosols such as fog, snow and rain and black carbon particulates present in the atmosphere are wavelength dependent and give rise primarily to attenuation / extinction of optical wave [3]. Especially for short links heavy fog is the main factor that limits the link function. For link lengths exceeding several hundred meters, *Index of refraction fluctuations lead to irradiance fluctuations* (refractive index turbulence (IRT)), *beam spreading and loss of spatial coherence* of the optical wave, thereby posing a severe problem at the receiver end.

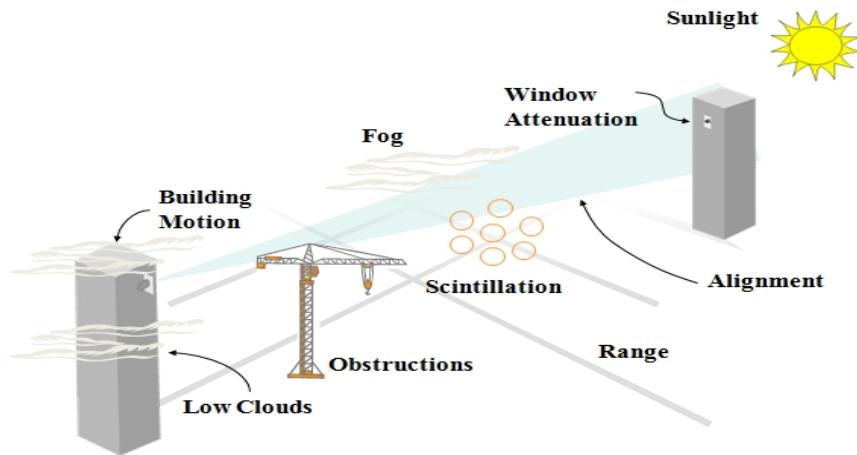


Figure 4.1: Various Channels effects affecting performance of FSO Link

**4.2 Diffraction** Is a natural wave phenomenon of all light waves which causes Beam Spreading of the wave as it propagates, which reduces the amount of energy within any given spot size inside the beam diameter [8]. The amount of beam spreading due to pure diffraction depends on the wavelength ‘ $\lambda$ ’ of the optical wave, shape of the phase front (i.e, spherical, uniform, etc.) and size of emitting aperture. The Beam Spot Size along the direction of propagation path has its minimum value at the Beam waist and the amount of beam spreading at large distances from the beam waist can be estimated by beam divergence angle,

$$\theta_B \cong \frac{\lambda}{\pi W_B} , \quad z \gg \pi \frac{W_B^2}{\lambda}$$

*Beam Waist =  $2W_B$*

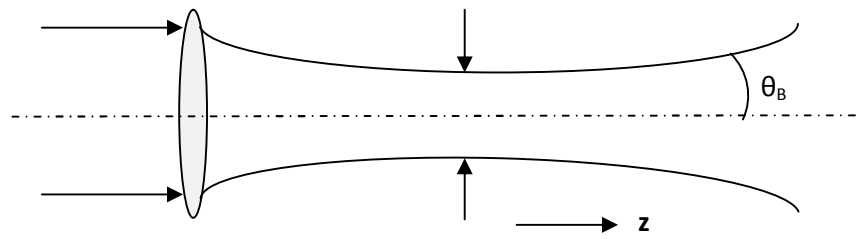


Figure 4.2: Far Field Divergence Angle

**4.3 Atmospheric Extinction Effects [3]** Clouds, rain, snow, fog, haze, pollution etc. are atmospheric factors that affect our viewing of distant objects. These same factors also affect the transmission of a laser beam through the atmosphere. Transmission through clouds or heavy fog or haze is normally not possible, because attenuation exceeds several tens of dB/km. However, the signal under clear-sky weather conditions is attenuated because of extinction caused by air molecules and aerosols. The transmittance ‘T’ of laser radiation that has propagated over a distance ‘L’ is described by the Beer’s law:

$$T = \exp (-\alpha_e(\lambda).L[Km])$$

The positive extinction coefficient  $\alpha_e(\lambda)$  describes the extinction level of the medium. The extinction is highly wavelength-dependent. Atmospheric trace gases lead to strong and broad absorption bands, each consisting of a multitude of fine absorption lines. Based on the spectral distribution of these bands, the atmospheric optical transmission windows with low signal losses of the propagating beam are calculated by evaluating thousands of absorption lines in the spectral range from 0.3  $\mu\text{m}$  to 14  $\mu\text{m}$ .

In addition to absorption, scattering should also be taken into account. This can be described by the Rayleigh scattering coefficient. Generally, scattering effects decrease monotonically with wavelength and altitude.

Fog consists of fine water droplets suspended in the air with diameters less than 100  $\mu\text{m}$ . It spontaneously induces decrease in visibility. Theoretically, fog exists when visibility is decreased to less than 1 km and the relative humidity of the air reaches the saturation level (relative humidity close to 100%). Fog is characterized by several physical parameters such as liquid water content, average particle size, particle size distribution and decrease in visibility.

There are different forms of light scattering and the main factor that determines the specifics of the scattering process is given by the ratio of the transmission wavelength compared to the size distribution of the scattering particles. In general terms, literature distinguishes between Rayleigh (particle size  $\ll$  wavelength), Mie scattering (particle size  $\sim$  wavelength), and geometrical scattering (particle size  $\gg$  wavelength). For all practical purposes Rayleigh scattering can be neglected for FSO systems operating in the near IR wavelength range.

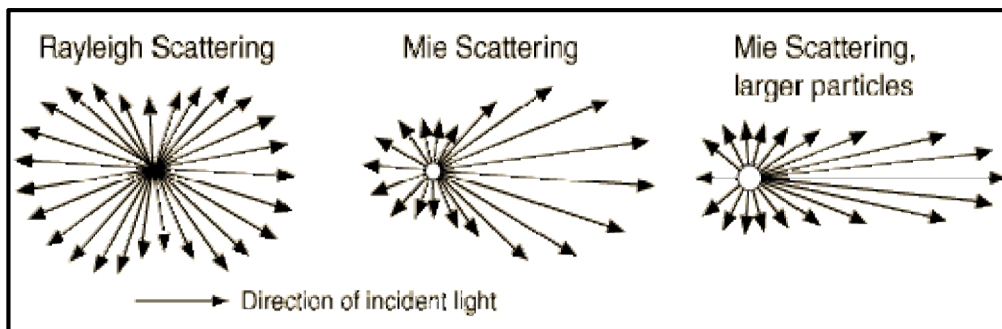


Figure 4.3: Scattering Effects

Due to lack of sufficiently detailed information at every installation site and complexity involved in Mie scattering theory, the models predicting the specific attenuation in terms of visibility were developed [9]. The models Kruse and Kim use this approach and predict specific attenuation using visibility.

A rough estimate for the clear-sky extinction is based on the Metrologic parameter visibility 'V', defined as the distance to an object where the image contrast drops to 2% of what it would be if the object were nearby instead (Taking **Mie scattering** into account).

**4.3.1 Kruse Relation Model for quantifying atmospheric extinction effects** The **Kruse relation model**, which is modified to reflect the attenuation in decibel per kilometer, is given by:

$$A_e \left[ \frac{dB}{Km} \right] = \frac{17}{V[Km]} \left( \frac{0.55}{\lambda (\mu m)} \right)^q \geq 0$$

Where, exponent ‘q’ is given by

$$q = \begin{cases} 1.6, & \text{if } V > 50 \text{ Km} \\ 1.3, & \text{if } 6 \text{ Km} \leq V \leq 50 \text{ Km} \\ 0.585.V^{1/3}, & \text{if } V < 6 \text{ Km} \end{cases}$$

MATLAB Simulation for Visibility conditions ranging from 0 Km to 70 Km for three different wavelengths is presented in the Figures 4.4 and 4.5 for better understanding and appreciation of Attenuation (in dB/Km) expected while designing the link under specific visibility condition posed by the environment.

Assuming,

1. Visibility,  $V = 1 \text{ Km}$ . For operating wavelength,  $\lambda = 1.55 \mu\text{m}$   
 $A_e \text{ (dB/Km)} = 17 \times (0.55/1.55)^{0.585} = \mathbf{9.2729 \text{ dB/Km}}$
2. Visibility,  $V = 1 \text{ Km}$ . For operating wavelength,  $\lambda = 0.532 \mu\text{m}$   
 $A_e \text{ (dB/Km)} = 17 \times (0.55/0.532)^{0.585} = \mathbf{17.334 \text{ dB/Km}}$

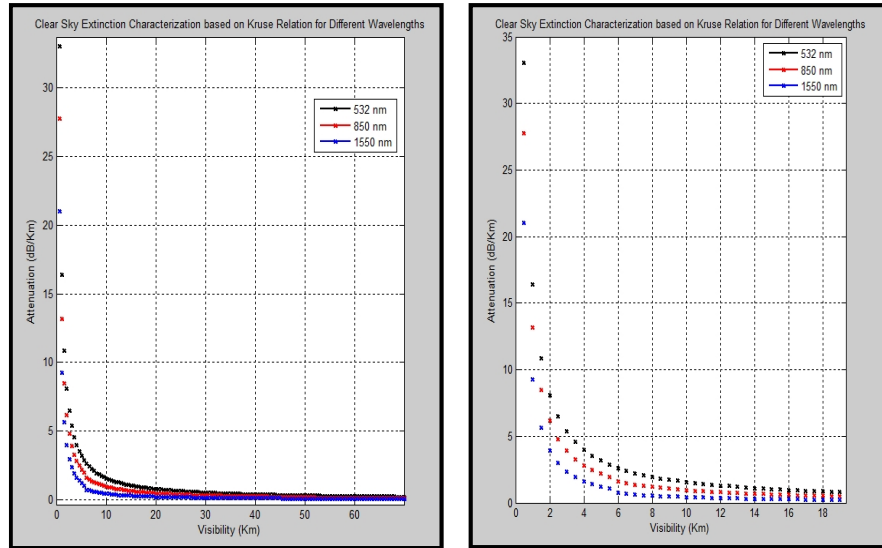


Figure 4.4: Simulation Results based on Kruse Model of Atmospheric Extinctions

Hence, Atmospheric Extinction Effects, as a result of Atmospheric Attenuation and Scattering processes (**based on Kruse Model**) would amount to a Transmission loss of **9.2729 dB/Km** at operating wavelength **1550 nm** and **17.334 dB/Km** at operating wavelength **532 nm**, respectively.

#### 4.3.2 Kim Relation Model for quantifying atmospheric extinction effects

Another well known Model, used to characterize the atmospheric extinction effects due to attenuation and scattering is the **Kim Model**. Kim, in his proposed Model rejected wavelength dependent attenuation for low visibility in dense fog.

$$q = \begin{cases} 1.6, & \text{if } V > 50 \text{ Km} \\ 1.3, & \text{if } 6 \text{ Km} \leq V \leq 50 \text{ Km} \\ 0.16V + 0.34 & \text{if } 1 \text{ Km} \leq V < 6 \text{ Km} \\ V - 0.5 & \text{if } 0.5 \text{ Km} \leq V < 1 \text{ Km} \\ 0 & \text{if } V < 0.5 \text{ Km} \end{cases}$$

Assuming,

1. Visibility,  $V = 1 \text{ Km}$ . For operating wavelength,  $\lambda = 1.55 \mu\text{m}$   
 $q = 0.16V + 0.34 = 0.5$   
 $A_e \text{ (dB/Km)} = 17 \times (0.55/1.55)^{0.5} = \mathbf{10.1266 \text{ dB/Km}}$
2. Visibility,  $V = 1 \text{ Km}$ . For operating wavelength,  $\lambda = 0.532 \mu\text{m}$   
 $q = 0.16V + 0.34 = 0.5$   
 $A_e \text{ (dB/Km)} = 17 \times (0.55/0.532)^{0.5} = \mathbf{17.285 \text{ dB/Km}}$

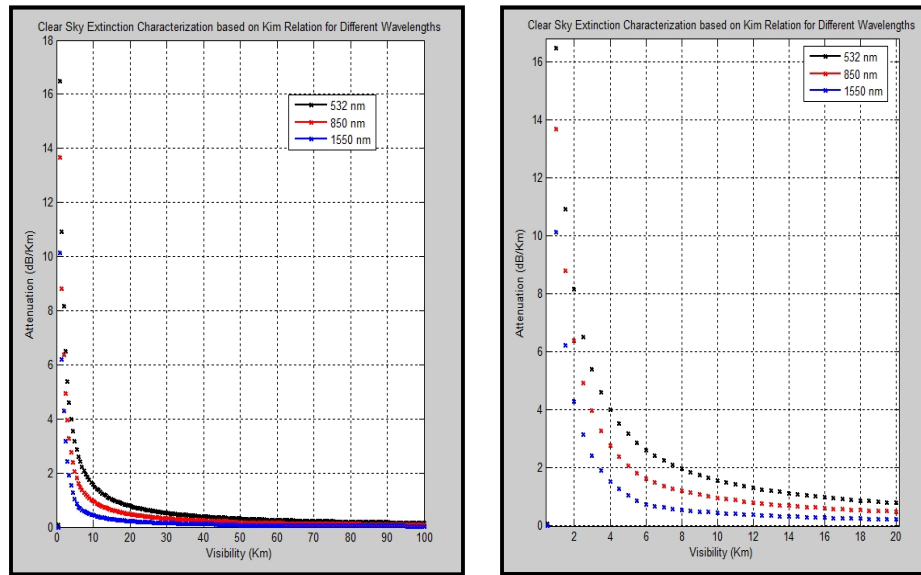


Figure 4.5: Simulation Results based on Kim Model of Atmospheric Extinctions

Hence, Atmospheric Extinction Effects, as a result of Atmospheric Attenuation and Scattering processes (**based on Kim Model**) would amount to a Transmission loss of **10.1266 dB/Km at operating wavelength 1550 nm and 17.285 dB/Km at operating wavelength 532 nm**, respectively.

**Note.** The above mentioned models give us a fair understanding as to how much attenuation is expected under varying Visibility conditions which must be carefully taken into account while calculating the link budget for Free Space Optical Communication. Experimental quantification of Atmospheric Extinction Effects is discussed in para 5.11.

**4.4 Influence of Atmospheric Turbulence** Atmospheric Turbulence is primarily generated by a temperature differential between Earth's surface and atmosphere [3], [8]. During daytime, the Earth is hotter than air, causing the air nearest to the ground / surface to be hotter than that above. Wave front distortions in the optical wave induced by atmospheric turbulence result in *beam spreading* (beyond pure diffraction), random variations of the position of the beam centroid called *beam wander* and a random redistribution of the beam energy within cross section of the beam leading to *irradiance fluctuations / scintillations*. In addition, atmospheric turbulence gradually destroys the *spatial coherence* of a laser beam as it propagates through the atmosphere. This loss of spatial coherence limits the extent to which laser beams may be collimated or focused, resulting in significant power level reductions in optical communication systems.

Random Fluctuations in the refractive index of the atmosphere are directly associated with microscopic temperature fluctuations caused by turbulent motion of the air due to winds and convection, leading to Optical Turbulence, thus making their cumulative effect on the optical wave quite profound.

The behaviour of this optical turbulence can be ascertained in a statistical manner [10]. Theoretical studies concerning optical wave propagation through optical turbulence are typically classified into *weak fluctuations or strong fluctuations*. These fluctuations are usually quantified by means of *Rytov Perturbation Approximation* [8], yielding relatively simple mathematical models for statistical quantities involving wave field.

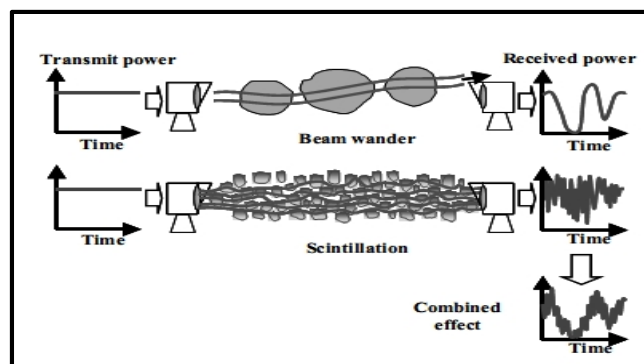


Figure 4.6: Effect of Atmospheric Turbulence



#### **4.4.1 Physical Effects of Optical Beam Propagation through Random Media**

Random variations of the refractive index, also known as index-of-refraction turbulence (IRT) - of the Earth's atmosphere are responsible for wavefront distortion [3]. Thus, if a beam with a longitudinal coherence length of several wavelengths propagates through IRT, the intensity of the original beam profile is redistributed. For example, a Gaussian-shaped intensity profile is transformed into a random interference pattern, called intensity speckle pattern.

As the refractive index structure along the path is time dependent because of the turbulent mixing of refractive index cells, the spatial intensity distribution at the receiver plane varies. The temporal variation of intensity observed at an infinitely small point and the spatial variation of intensity within the receiver aperture are commonly described as “**Scintillation**”.

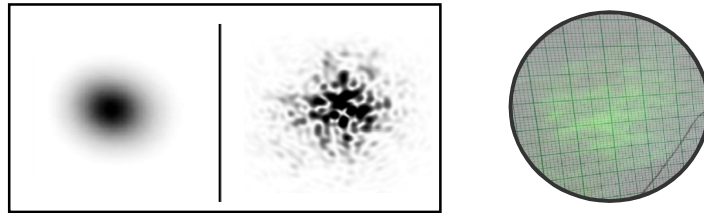


Figure 4.7: Laser beam propagation through turbulent atmosphere: Intensity cross-section of the transmit beam (left), intensity cross-section at the receiver plane experimentally observed (right)

## CHAPTER 5

### EXPERIMENTAL QUANTIFICATION OF CHANNEL EFFECTS USING 532 nm LASER SOURCE

Due to non availability of funds while undertaking the project of establishing FSO link at 1550 nm, the project scope was redefined to characterize and quantify all atmospheric channel effects with a commercially available Green Laser Source and analyze and predict the aforesaid effects at a link range of 1 Km. The project was undertaken in the following sequence:

#### 5.1 Determining Exact Wavelength of the emitting Laser

For the scope of the project, a commercially available Green Laser was purchased off the shelf in order to characterize effects of atmospheric Turbulence. In order to ascertain the exact optical wavelength emitted by the LASER, the spectral irradiance pattern of the LASER was tested on LightMtrX (by Latsphere).

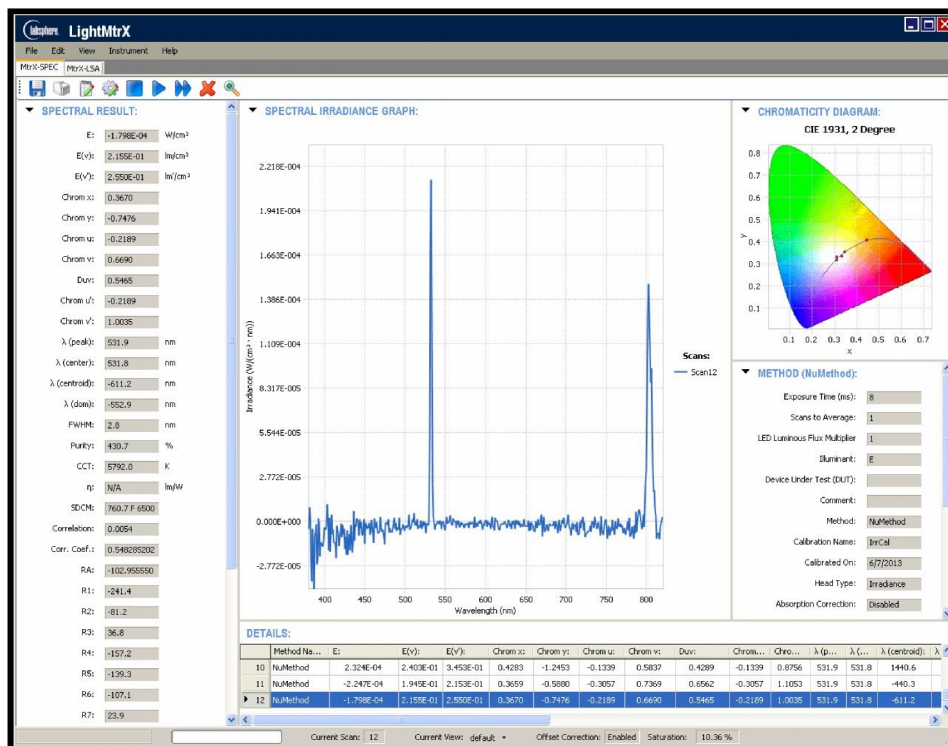


Figure 5.1: Optical wavelength Measurement using LightMtrX

From the Spectral Irradiance Graph, it was found that the optical wavelength of the Green Laser is ' $\lambda$ ' = 531.8 nm. We also clearly observe a prominent irradiance at IR wavelength of 808 nm.

The main reason behind 808 nm wavelength is the presence of high residue of a powerful (>200 mW) 808 nm IR GaAlAs laser diode which pumps a neodymium-doped yttrium aluminium garnet (Nd:YAG) or a neodymium-doped yttrium orthovanadate (Nd:YVO<sub>4</sub>) crystal which further produces 1064 nm wavelength light from the main spectral transition of neodymium ion. This light is then *frequency doubled* using a nonlinear optical process in a KTP (Potassium Titanyl Phosphate, KTiOPO<sub>4</sub>) crystal, producing 532 nm light. Green Lasers are usually around 20% efficient, although some lasers can reach up to 35% efficiency. In other words, a green Laser using a 2.5 W pump diode would be expected to output around 500-900 mW of 532 nm light. Hence, we observe a strong presence of remnants of 808 nm IR Pump in the Spectral irradiance graph.

## 5.2 Determining Beam Profile of the emitting Laser

In order to ascertain the Beam Profile of the emitting LASER, Laser-Cam-HR-UV (by Coherent) was used and the experiment was carried out under negligible ambient light conditions at two different spatial states of the emitting diode.

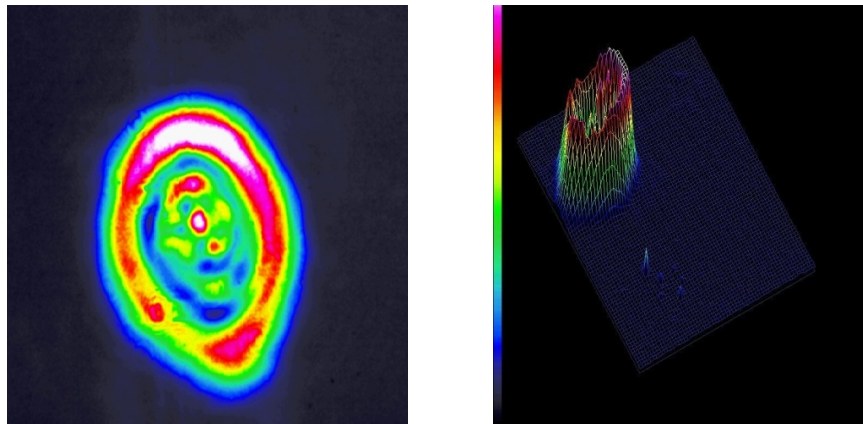


Figure 5.2: Beam Profile for a collimated Beam - 531.8 nm

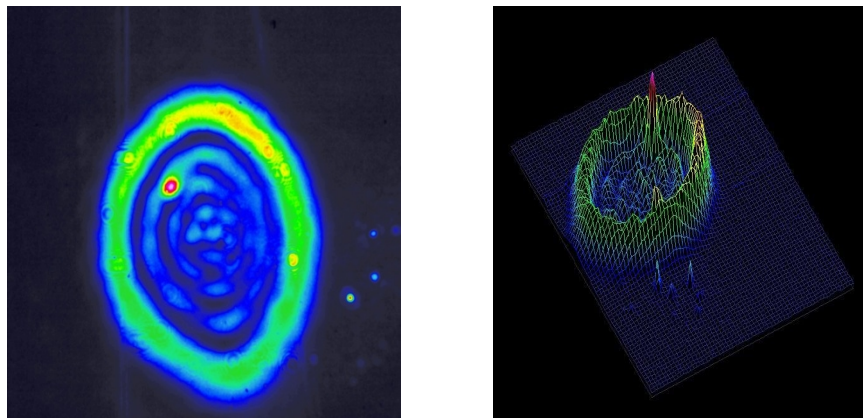


Figure 5.3: Beam Profile for a divergent Beam - 531.8 nm

The Beam Profile resembles higher order *Laguerre-Gaussian Beams* [8] having higher order TEM<sub>11</sub> (multimode).

### 5.3 Beam Divergence Profile – 531.8 nm Laser Source

This experiment was initially carried out to ascertain the Beam Divergence Profile of the Laser Source.

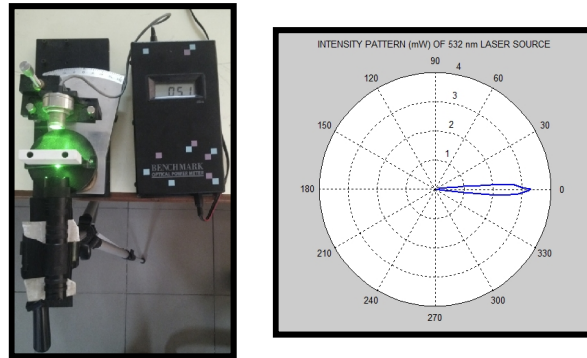


Figure 5.4: Narrow Beam Divergence – Laser Source

### 5.4 Determining Divergence Angle ' $\theta_B$ ' of the Laser Beam

Beam Divergence angle was quantified by carrying out lateral conversion of the beam diameter on a graph sheet at varying distance.

Ser No	Distance (mm)	Time	Temp	Humidity	Wind Speed	Expt Duration	Inner Beam Dia (mm)	Beam Radius (mm)	Angle
1	46000	1845 Hrs	26° C	60%	0 ° N 18 Kmph	15 Min	156	78	<b>0.0971</b>
2	75000	1855 Hrs	26° C	60%	0 ° N 18 Kmph	15 Min	255	127.5	<b>0.0974</b>
3	100000	1905 Hrs	26° C	60%	0 ° N 18 Kmph	15 Min	340	170	<b>0.0974</b>

Table 5.1: Experimental Quantification of Half Angle of Beam Divergence ( $\theta/2$ )

It was experimentally ascertained that the *divergence Beam Half Angle of the LASER under test is 0.097°* (Approx) = 0.00169 rad = 1.692 mrad.

Beam spot radius at 1 Km distance from Transmitter (based on divergence Beam Half Angle = 0.097°)  $\approx$  **1.6929 m**

We know by theory of Diffraction ((Refer para 4.2),

$$\theta_B \cong \frac{\lambda}{\pi W_B} , \quad z \gg \pi \frac{W_B^2}{\lambda}$$

For  $\lambda = 531.8 \text{ nm}$  and  $\theta_B = 1.692 \text{ mrad}$ , respectively.

**Beam Radius at waist,  $W_B \approx 0.000100 \text{ m} = 0.10046 \text{ mm}$**

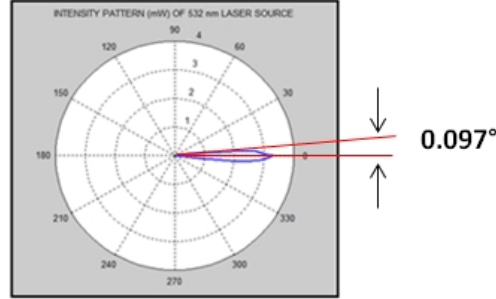


Figure 5.5: Beam Divergence Angle

## 5.5 Optical Receiver for FSO Link

FSO Communication system established for the scope of the project is based on **direct Detection** Scheme [8] at Receiver end. In Direct (incoherent) Detection, the information is transmitted at base-band, demodulated at the Receiver back into the transmitted signal. This system has following characteristics:

- (a) It responds only to the instantaneous power of collected field.
- (b) Receiving lens focuses the optical signal onto a photo-detecting surface.
- (c) Photo-detector converts the focused optical field into an electrical signal for processing.

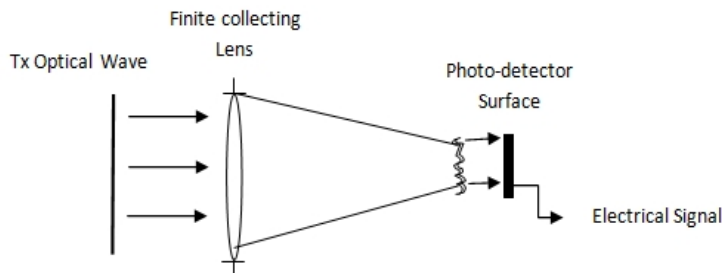


Figure 5.6: Direct Detection System Schematic

The modulation format for transmitted signal is essentially **intensity modulation**. Noise sources present throughout the Rx include:

- (a) Background Radiation (Sun).
- (b) Detector Noise or Shot Noise.

- (c) Circuit and Electronic Noise after photo-detection.

**Note:**

- (a) If the Rx aperture in the presence of atmospheric turbulence is smaller than the correlation width of the irradiance fluctuations on the Received signal, the system behaves essentially like a ‘point receiver’. Here, turbulence induced signal fluctuations are quite deleterious to system performance.
- (b) Increasing the aperture diameter beyond irradiance correlation width increases the average signal level and also simultaneously reduces fluctuation level in the received signal due to *Aperture Averaging* [10].

In order to take advantage of Aperture averaging effect while establishing a robust FSO link range  $> 100$  m, a spotterscope having objective diameter of 50 mm has been used as Telescope at the Receiver end. This Telescope is further integrated to the Photo-detector in Free Space ahead of the focal length of the eye piece of the Telescope so as to allow a larger spot to be made at the Photo-detector end in order to ensure that at any point of time the Photo-detector receives suitable intensity of Tx signal.

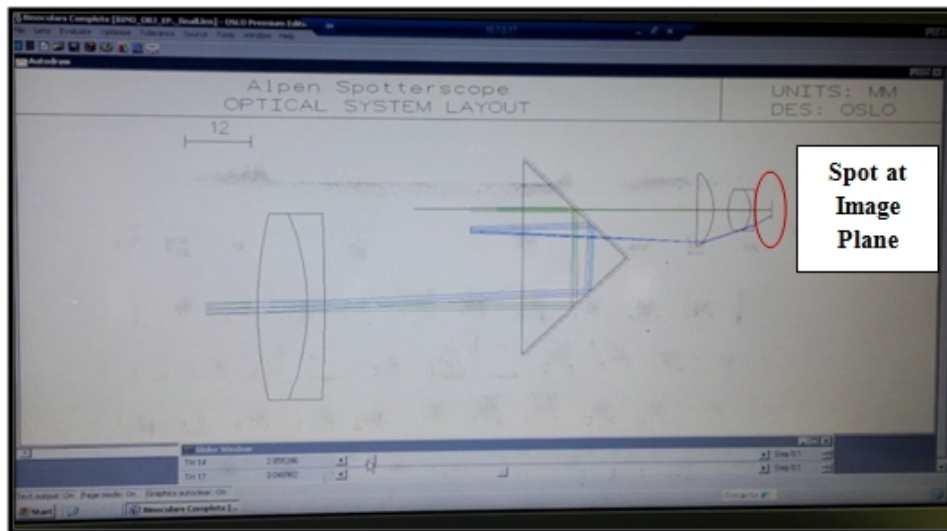


Figure 5.7: Simulation and Analysis of Integration of Spotter scope with Photo-detector, understanding the advantage of having a Beam Spot at Image Plane,  
Software used – OSLO Premium Edition



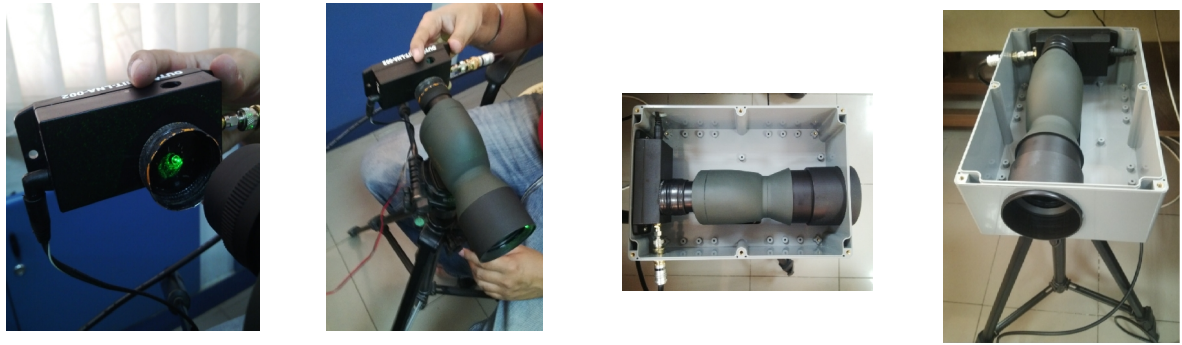


Figure 5.8: Integration of Spotter scope with Photo-detector - Direct Detection System for FSO Link

## 5.6 Optical Transmitter for FSO Link

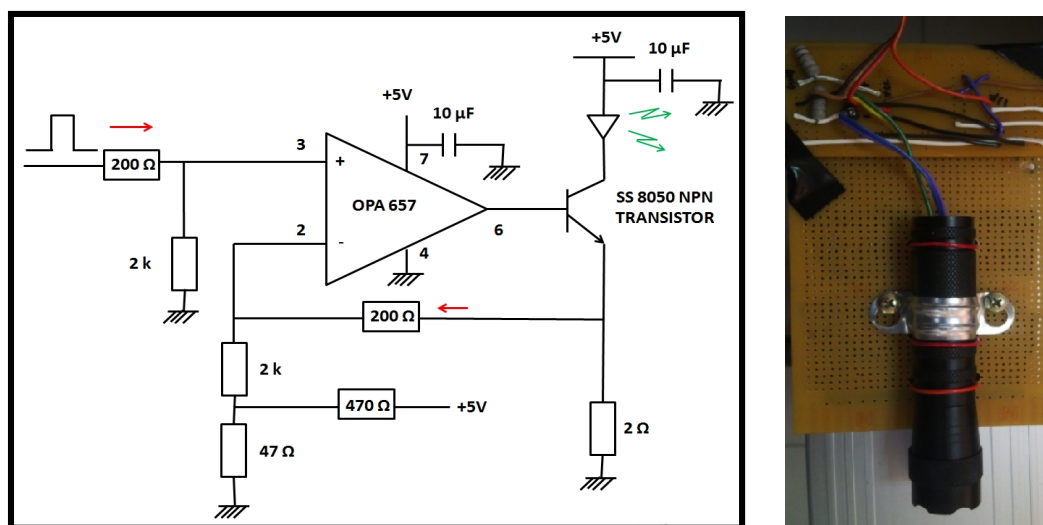


Figure 5.9: Circuit Diagram - Driver for LASER for direct Modulation

Post integration of Telescope with Photo-detector and establishing Robust Receiver setup, an electronic driver circuit (Figure 5.9) was worked out in order to carry out direct modulation of the CW Laser externally in order to achieve on-off keying for transmission of data at defined Bit Rates.

## 5.7 Link Bandwidth

A necessary requirement in the design of any communication system is the Bandwidth, which is a measure of how rapidly the information bearing portions of the signal can change.

FSO Link was set up on the IIT Madras, Electrical Department Rooftop to experimentally ascertain the Link performance by quantifying the Link Bandwidth at 100m under normal atmospheric / weather conditions, by carrying out experiment based on direct modulation of

LASER Diode with the transmitter circuit (fabricated with OPA 657). The link was successfully setup. Link Bandwidth was restricted to 1.122 MHz, mainly because we are interested in quantifying atmospheric effects affecting the performance of FSO link with ‘ $\mu$ sec’ variations. Scintillations primarily occur in ‘ $\mu$ sec’ variations, whereas effects of beam wander are expected to occur in ‘msec’ variations [10]. (Here, Sinusoidal wave was transmitted from the Arbitrary Waveform generator). Finally, a Random Bit Sequence was transmitted via Lab View (on Computer) interfaced with arbitrary waveform generator at the Transmit end. The same was received at the receiver end with negligible probability of error.

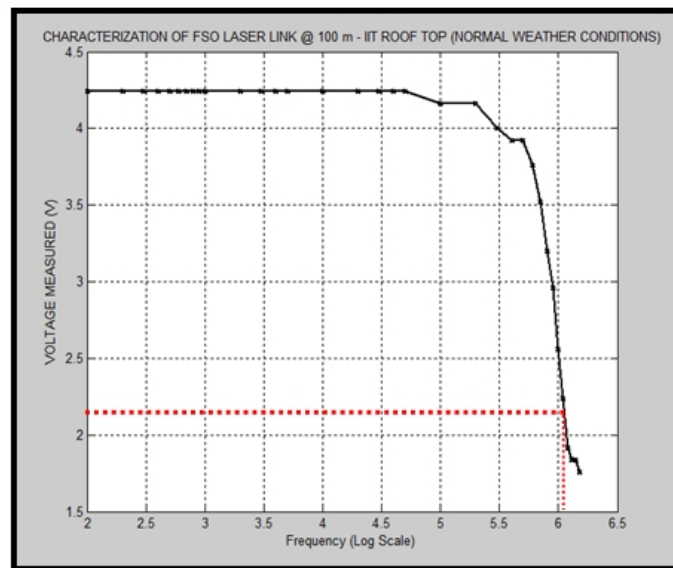


Figure 5.10: Link Bandwidth

## 5.8 Establishing FSO Link – Link Range 100 m



Figure 5.11: FSO Link Setup - Transmitter End



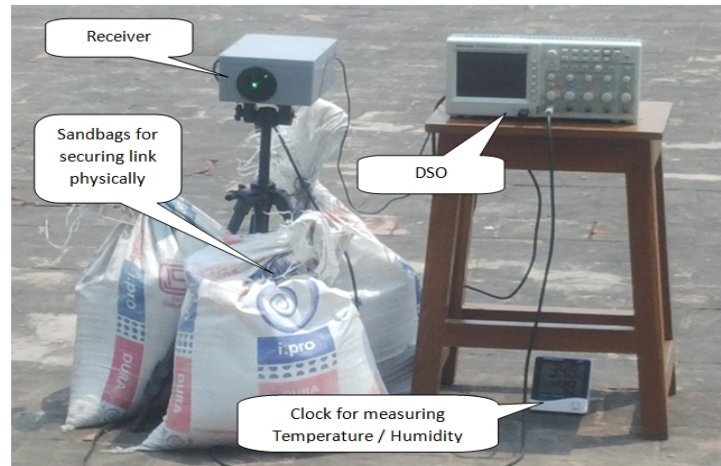


Figure 5.12: FSO Link Setup - Receiver End

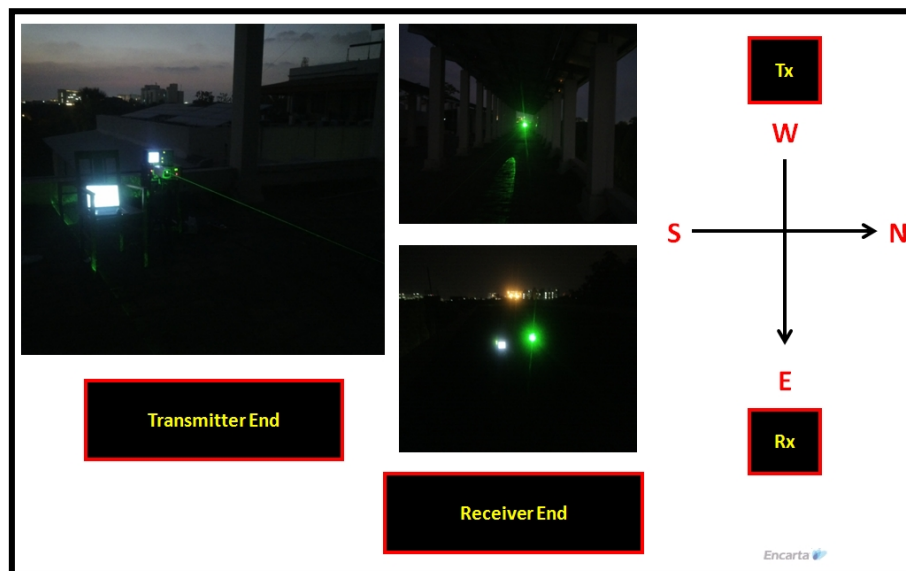


Figure 5.13: FSO Link Setup - 100 m

### 5.9 Characterising Traversing angle along Central Axis

This experiment is essential in order to understand as to how much Angular Freedom the receiver enjoys with the present configuration.

From the experimental result, it was ascertained that the receiver arrangement can be traversed through  $\pm 3^\circ$  while being aligned along the central axis with the transmitter. This implies that even if the transmit Beam would wander by an angle of  $\pm 3^\circ$  (due to Temporary pointing misalignment or Beam Wander), optical power could still be captured by the collecting lens of the telescope.

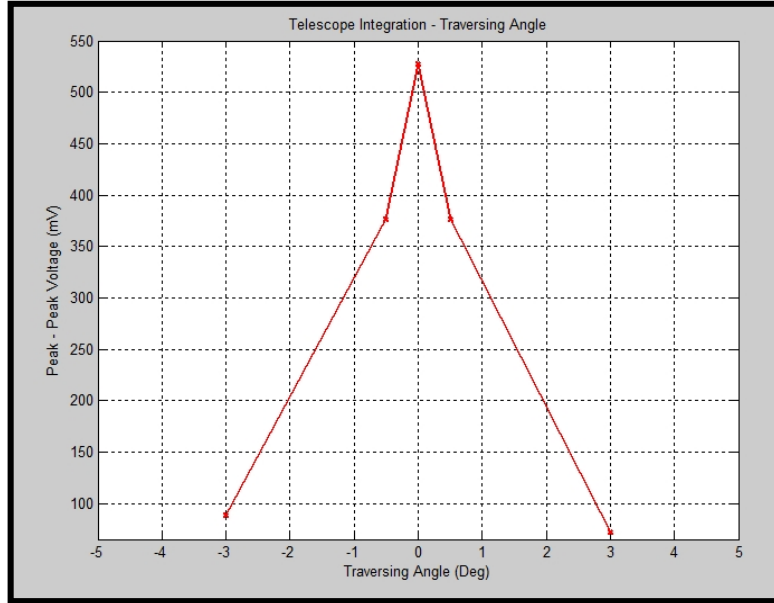


Figure 5.14: Freedom of Alignment along Traversing Angle

### 5.10 Power collected at the Receiver due to Background Radiation (Sun)

This was measured in the absence of any kind of direct optical Transmission from the Transmitter end.

Shift in DC Level observed at DSO in Presence of solar radiation: 355 mV

Hence,  $I_p = V/R = 355 \text{ mV} / 10 \text{ K}\Omega = 35.5 \text{ }\mu\text{A}$

$P_{in} = I_p / \text{Responsivity} = 35.5 \times 10^{-6} / 0.8 = 44.375 \text{ }\mu\text{W} \approx 45 \text{ }\mu\text{W}$

The effect of Solar radiation on the photo-detector can be suitably negated by using optical filters in front of receiver telescope arrangement, thereby allowing only transmit wavelength to reach the receiver end via free space photo-detector.

### 5.11 Atmospheric Extinction Effects

Experiment was carried out with the help of Auto Digital Lux Meter V6610 at two different times of the day at a link range of 250 m. Here, we have assumed negligible Pointing Error.

Lux to watts calculation with area in square meters [11], [12]

The power  $P$  in watts (W) is equal to the illuminance  $E_v$  in lux (lx) times the surface area  $A$  in square meters ( $\text{m}^2$ ), divided by the luminous efficacy  $\eta$  in lumens per watt (lm/W):

$$P_{(W)} = E_{v(lx)} \times A_{(m^2)} / \eta_{(lm/W)}$$

Luminous Efficacy in Lumens/W for 532 nm = **609.5 lm/W**;  $A = 8.8 \text{ mm}$

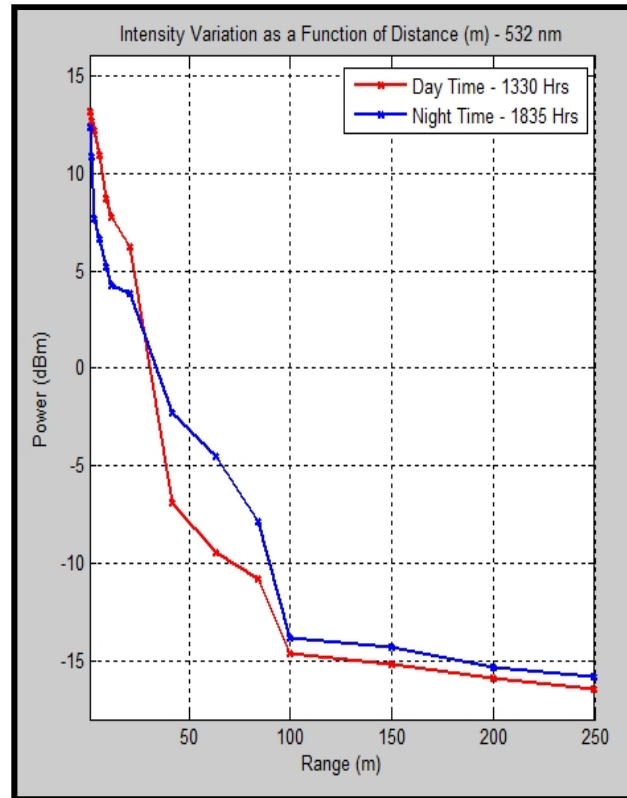


Figure 5.15: Experimental Quantification of Atmospheric Extinction (Link Range 250 m)

#### 5.11.1 Expected Atmospheric Extinction Effects - Extrapolated to Link range 1000 m

Atmospheric extinction effects based upon above observations were now extrapolated for a link range of 1000 m. It was suitably predicted that expected attenuation of the FSO link (link range 1 Km) at day time is 39 dB/Km and at night time is 34 dB/Km.

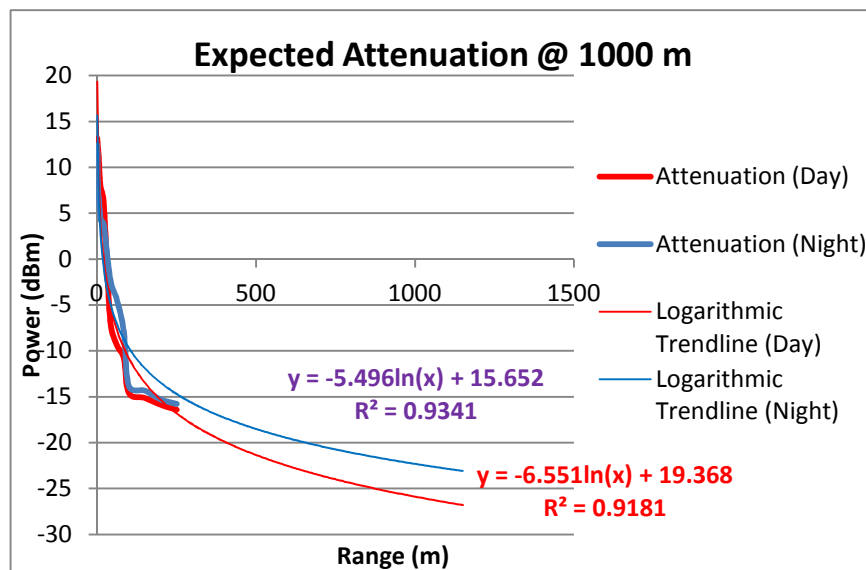


Figure 5.16: Analysis and extrapolation of Atmospheric Extinction (Link Range 1000 m)

Attenuation per Km is very high owing to the presence of Black Carbon particles along with aerosols in the atmospheric channel which lead to very high absorption and scattering of the beam encountered.

Theoretically, Attenuation due to Atmospheric Extinction for high visibility,  $V = 1$  Km, for operating wavelength,  $\lambda = 0.5318 \mu\text{m}$  is quantified as under (Refer Para 4.3)

$$A_e (\text{dB/Km}) = (17) \times (0.55/0.5318)^{0.585} = \mathbf{17.334 \text{ dB/Km}}$$
 (Based on Kruse Model)

$$A_e (\text{dB/Km}) = (17) \times (0.55/0.5318)^{0.5} = \mathbf{17.289 \text{ dB/Km}}$$
 (Based on Kim Model)

However, while theoretically analyzing these models, we only consider presence of aerosols in the channel and do not take into account presence of pollutants like black carbon particles having very high beam absorption and scattering properties. Hence, experimental values of Atmospheric Extinction are higher than simulation results.

#### **5.11.2 Attenuation and Scattering Characterisation – Moderate Fog conditions,**

##### **Visibility 350 m**

Experiment was carried out with the help of Auto Digital Lux Meter V6610 for a distance of 100 m in New Delhi. Here, we have assumed negligible Pointing Error. (Appx 'B')

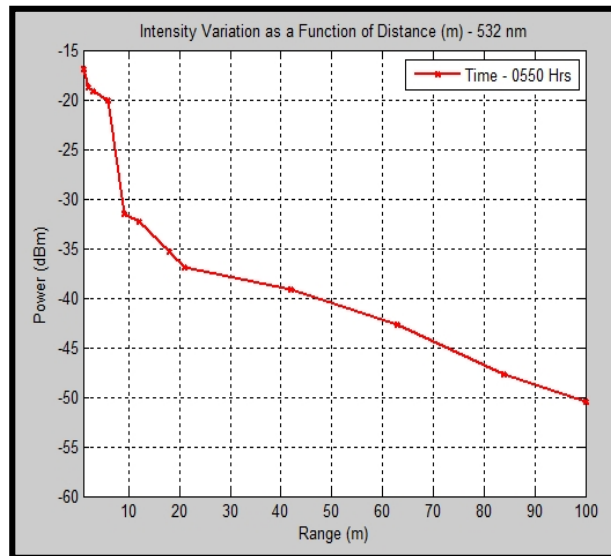


Figure 5.17: Experimental Quantification of Atmospheric Extinction – Moderate Fog conditions, Visibility – 350 m (Link Range 100 m)

#### **5.11.3 Expected Atmospheric Extinction Effects, Fog - Extrapolated to Link range 1000 m**

Atmospheric extinction effects based upon above observations were now extrapolated for a link range of 1000 m. It was suitably predicted that

expected attenuation of the FSO link (link range 1 Km), under moderate Fog conditions, visibility 350 m is **48.18 dB/Km**.

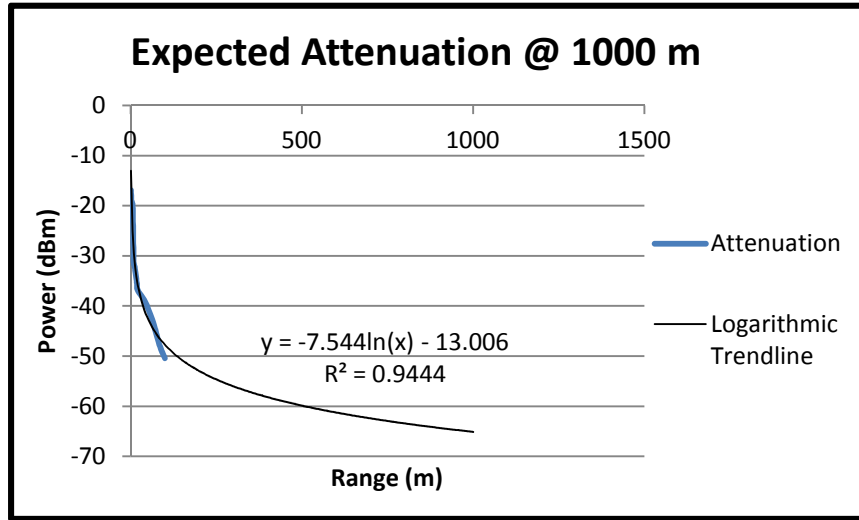


Figure 5.18: Analysis and extrapolation of Atmospheric Extinction - Moderate Fog conditions, Visibility – 350 m (Link Range 1000 m)

Based upon Kruse and Kim Models of Atmospheric extinction, (as discussed in para 4.3), Attenuation due to Atmospheric Extinction for visibility,  $V = 350\text{m}$ , for operating wavelength,  $\lambda = 0.5318 \mu\text{m}$  is quantified as under:

$$A_e \text{ (dB/Km)} = (17/0.35) \times (0.55/0.5318)^{0.585} = \mathbf{49.53 \text{ dB/Km}} \text{ (Based on Kruse Model)}$$

$$A_e \text{ (dB/Km)} = (17/0.35) \times (0.55/0.5318)^0 = \mathbf{48.57 \text{ dB/Km}} \text{ (Based on Kim Model)}$$

It can be clearly inferred that under dense fog, atmospheric channel experiences dense concentration of Aerosols and water molecules. Above experimental values nearly match the simulated values of universally recognized models for quantification of atmospheric extinction.

## 5.12 Atmospheric Turbulence

### 5.12.1 Kolmogorov Theory of Turbulence

Considering the atmosphere as a viscous fluid, it has two distinct states of motion – Laminar and turbulent. Mixing of air does not occur in **Laminar Flow** for which the velocity flow characteristics are uniform or change in some regular fashion. In case of **Turbulent Flow**, the velocity field loses its uniform characteristics due to dynamic mixing and acquires random subflows called **turbulent eddies** [8].

By Reynolds similarity theory, a non dimensional quantity  $Re = Vl/v$ , referred to as **Reynolds number**. Here, ‘V’ and ‘l’ are characteristic velocity and dimension of the flow and ‘v’ is the kinematic viscosity (in  $m^2/s$ ). The transition from laminar flow to turbulent motion takes place at a **critical Reynolds number**, above which the motion is considered turbulent.

**Note.** Close to the ground, characteristic scale size is 1~2 m, characteristic wind speed is 1-5m/s and  $v \sim 0.15 \times 10^{-4} m^2/s$ , leading to large Reynolds numbers on the order  $Re \sim 10^5$ . In these cases, motion is considered to be highly turbulent.

**5.12.2 Refractive Index Fluctuations** The index of refraction ‘n’ is one of the most significant parameters of the atmosphere for optical wave propagation. It is very sensitive to small scale temperature fluctuations. In particular, temperature fluctuations combined with turbulent mixing induce a random behaviour in the field of atmospheric index of refraction.

Index of **Refraction structure constant**,  $C_n^2 (m^{-2/3})$ , also known as **Structure Parameter**, is a measure of the strength of fluctuations in the refractive index [8]. Behaviour of  $C_n^2$  at a point along the propagation path can be deduced from temperature structure function obtained from point measurements. Values of  $C_n^2$  typically range from  $10^{-17} m^{-2/3}$  or less for “weak turbulence” and upto  $10^{-13} m^{-2/3}$  or more when the turbulence is “strong”. Over short time intervals at a fixed propagation distance and constant height above the ground, it may be reasonable to assume that  $C_n^2$  is essentially constant.

**5.12.3 Weak and Strong fluctuation conditions** In the study of spherical waves that have propagated over a path length ‘L’, it is important to distinguish between these cases by values of Rytov variance [8] (commonly denoted as measured variance)

$$\sigma_R^2 = 1.23 C_n^2 k^{7/6} L^{11/6}$$

Where,  $C_n^2$  is the refractive index structure parameter. Weak fluctuations are generally associated with  $\sigma_R^2 < 1$ . Rytov variance physically represents the irradiance fluctuations associated with an unbounded wave. Moderate fluctuation conditions are characterised by  $\sigma_R^2 \sim 1$ , strong fluctuations are associated with  $\sigma_R^2 > 1$ , and saturation regime is defined by condition  $\sigma_R^2 \rightarrow \infty$ .

Here, Wave Number,  $k = \frac{2\pi}{\lambda}$ , where,  $\lambda = 531.8 \text{ nm}$ . Hence,  $k = 0.01181 \times 10^9$

### 5.13 Quantifying effect of Atmospheric Turbulence

Free Space Optical Link was established on three different days for 24 hours in the following manner:

- (a) FSO link – Collimated Beam - 60 m (Link Distance)
- (b) FSO link – Divergent Beam (Overfilling Receiver Telescope Aperture) - 60 m
- (c) FSO link – Divergent Beam (Overfilling Receiver Telescope Aperture) - 100 m

#### **FSO link – Divergent Beam (Overfilling Receiver Telescope Aperture) – 100 m**

Transmit Beam was made to diverge from existing collimated state in order to overfill the Receiver Telescope Aperture and reduce the optical power received at the Receiver end so as to operate the LNA in linear regime in order to pick up random fluctuations in received signal to further quantify the effect of Optical Turbulence on the link established. Real time Data was collected at regular intervals of 15 minutes over a 24 hour cycle and a corresponding Histogram was plotted for each experiment. A second order Gaussian Fit was carried out on the Histogram in order to determine the corresponding mean and variance of the data collected at R-square  $\approx 0.99$ .

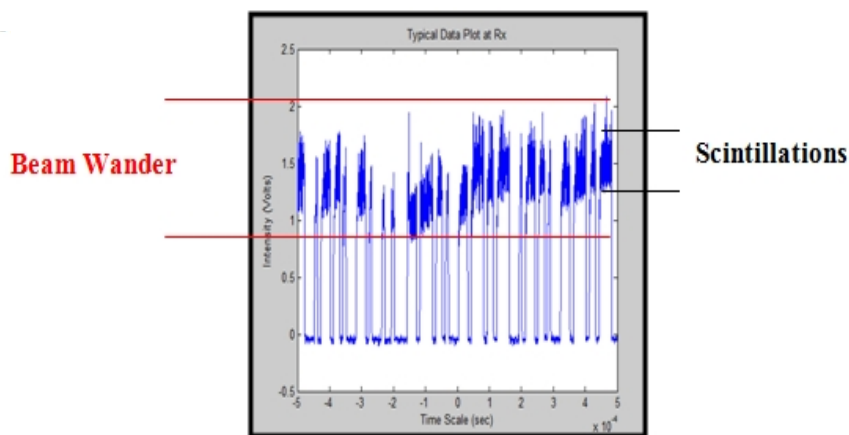


Figure 5.19: Typical Turbulent Distorted Data Plot observed at receiver depicting effect of Atmospheric Turbulence on transmitted data

Experimental Quantification and Analysis of Atmospheric Turbulence based on Histogram Plot over 24 Hour cycle is discussed in **Appx ‘C’** to the Thesis Report.

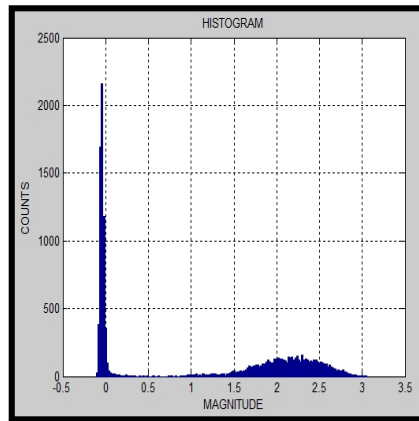


Figure 5.20: Typical Histogram plot based on data collected

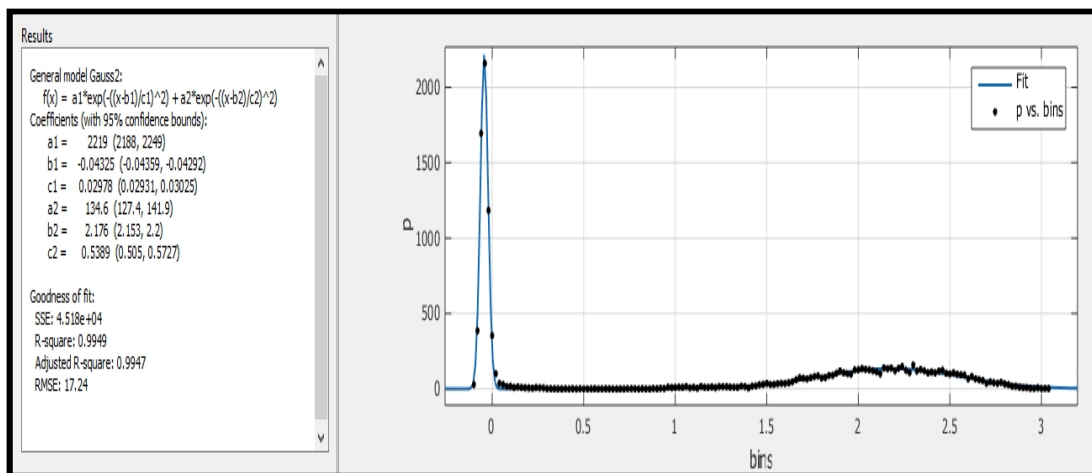


Figure 5.21: Gaussian Fit on Histogram

## 5.14 Observations and Analysis – Quantification of Atmospheric Turbulence

### 5.14.1 Correlation between Temperature and Humidity

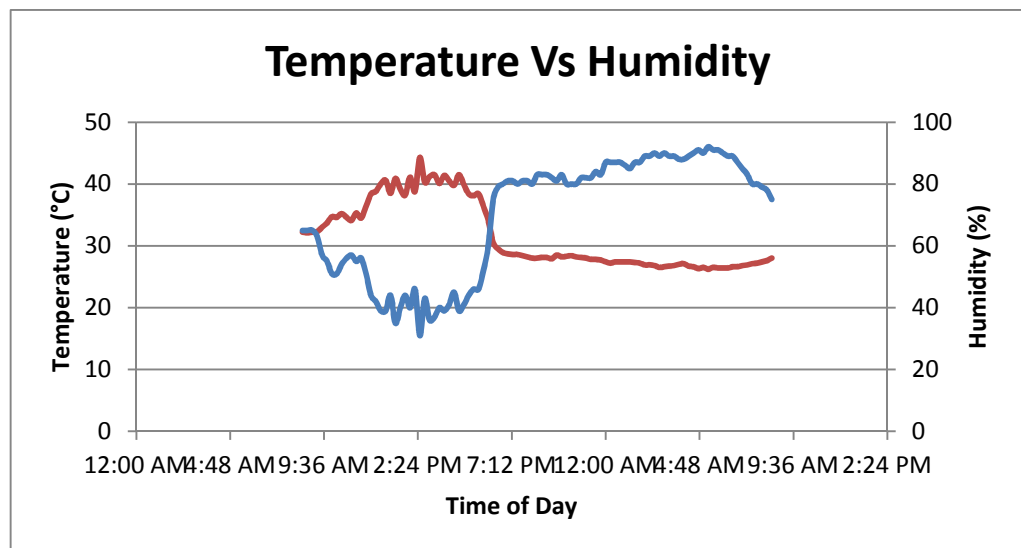


Figure 5.22: Correlation between Temperature and Humidity



Temperature and humidity were quantified over a 24 Hour Cycle and the same was plotted. Clear analysis of figure 5.22 indicates that Temperature and Humidity are inversely correlated with very high degree of correlation, i.e., as Temperature increases, Humidity decreases and vice versa. In day time, at afternoon hours, the temperature measured is the highest, which brings out that at this time of the day Humidity measured is lowest. Humidity tends to increase during the night hours.

#### 5.14.2 Correlation between Temperature and Windspeed

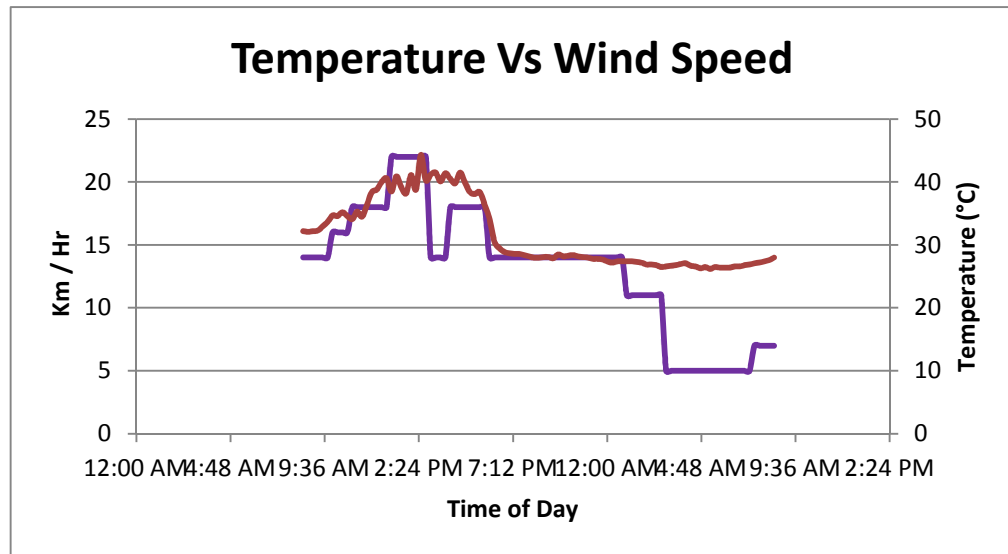


Figure 5.23: Correlation between Temperature and Windspeed

Very high turbulence in air, essentially during afternoon hours was observed. With increase in Temperature, Earth's surface experiences thermal looming, which in turn increases turbulence in air. Hence, we observe greater windspeed / turbulence in air in afternoon hours as compared to night hours, when the Earth's surface is comparatively cooler.

#### 5.14.3 Correlation between Variance (when '1' is transmitted) and Temperature, Windspeed

Variance of received data, when '1' is transmitted (Laser in ON State) is a result of both temperature and windspeed seen as two independent Random Processes. From figure 5.24, we can observe that during day time (afternoon hours), when the atmosphere is highly turbulent, due to high wind speed and thermal looming encouraging random movement of aerosols in the channel, fluctuations in variance tend to increase as a result of scintillations as well as beam wander leading to temporary pointing errors between the transmit beam and the receiver setup. During night hours as

the temperature is nearly constant we observe high correlation between speed of wind and variance of data received. (However, these fluctuations are minor in nature)

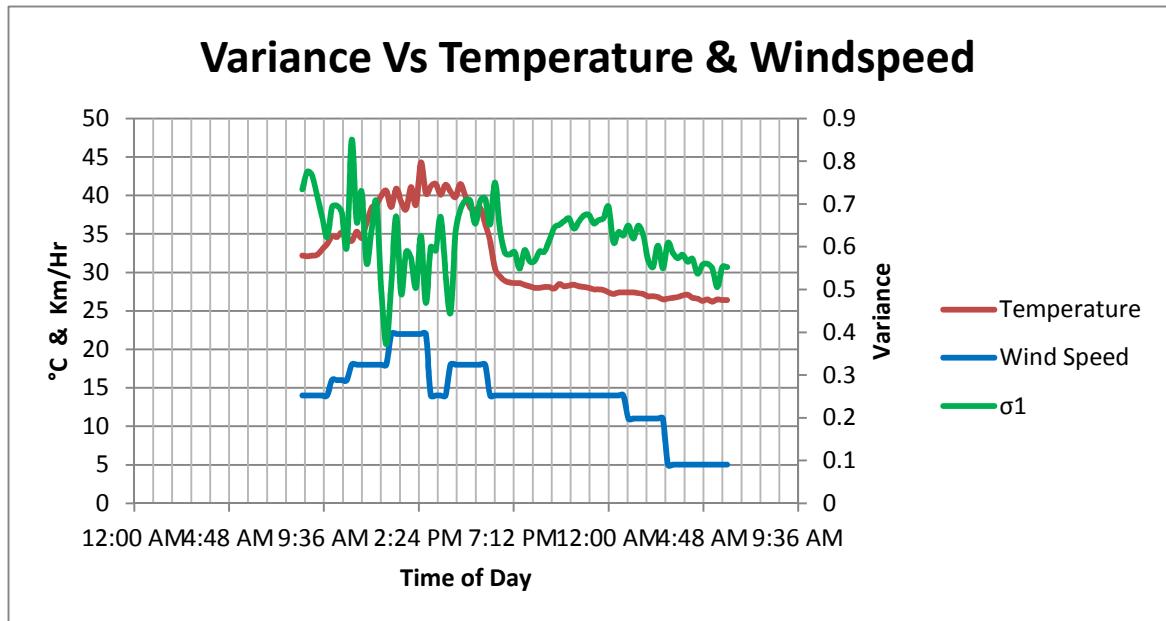


Figure 5.24: Effect of Temperature and Windspeed on Variance

We note that Variance is essentially high when Temperature is high (it is a combined effect of both Temperature and windspeed on Atmospheric Turbulence). However, when temperature is low / nearly constant, variance is primarily governed by variation in windspeed alone. Hence, effect of variance is low and nearly constant.

#### 5.14.4 Correlation between Mean (when '1' is transmitted) and Temperature, Windspeed

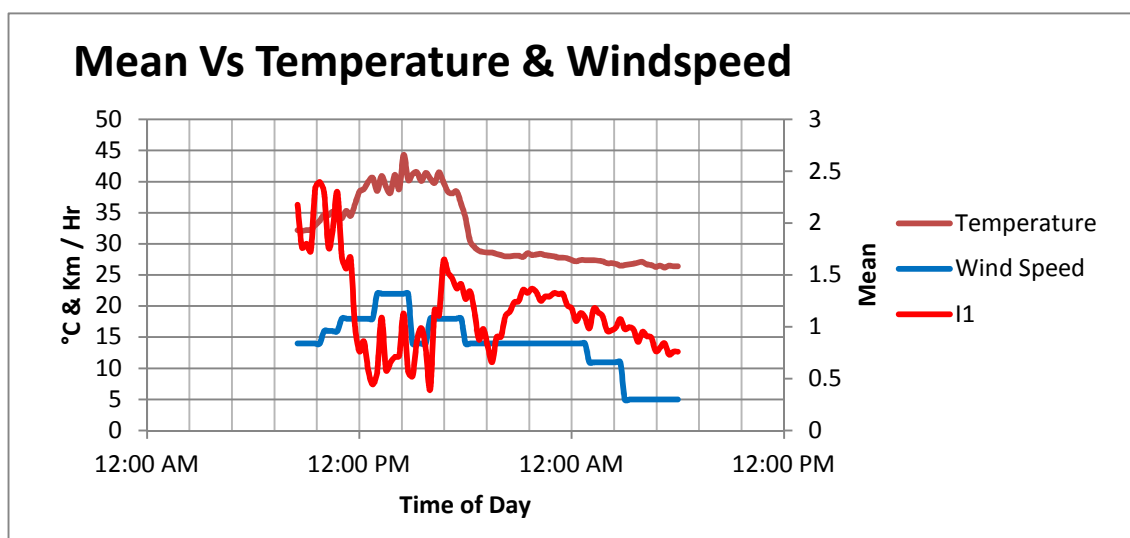


Figure 5.25: Effect of Temperature and Windspeed on Mean

Mean of received signal fluctuates with atmospheric Turbulence. During our observation, it was observed that at certain instances, mean falls down drastically as a result of temporary geometric misalignments in the FSO link primarily because the transmit beam has wandered off the line of sight course established with the receiver and the light intensity does not fall over the receiver at those instances. Mean is comparatively higher when there is low atmospheric turbulence, essentially during night hours.

#### 5.14.5 Correlation between Mean (when '1' is transmitted) and Variance

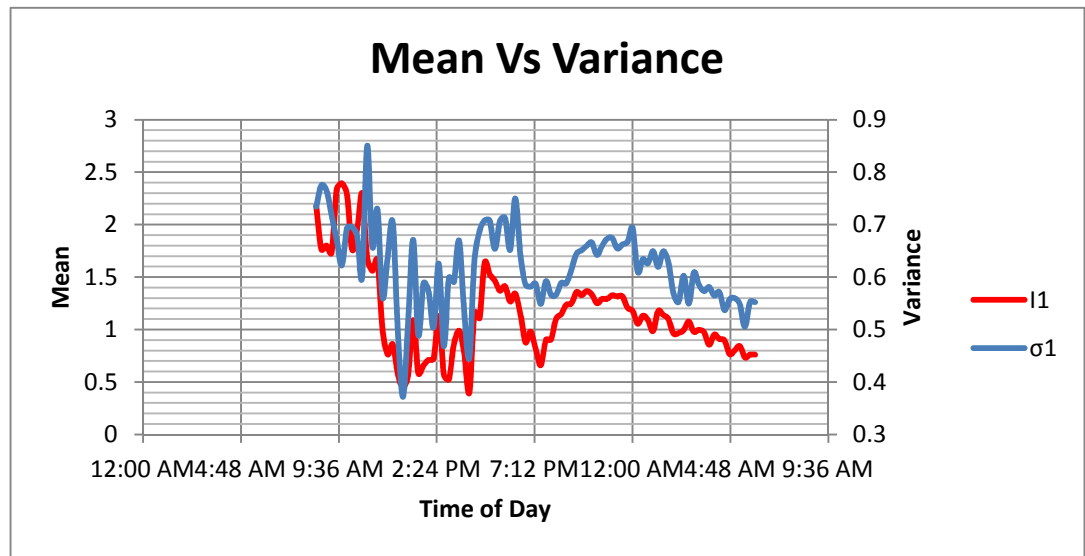


Figure 5.26: Correlation between Mean and Variance

We observe that when mean of the signal is very low as a result of temporary misalignments due to beam wander, not much can be commented about the variance of the signal arising out of scintillations as it is majorly governed by Beam Wander instead of index of refractive turbulence leading to scintillation effect. Hence, at low mean values, corresponding variance values are not reliable. When the value of mean is observed above a particular threshold, corresponding variance of signal is highly correlated with mean of the signal.

#### 5.14.6 Refractive Index structure parameter computed based on corresponding Variance

It was experimentally verified that Refractive Index Structure parameter  $C_n^2$  confirms with the Theoretical results as discussed in para 5.12.2. Based on the results

discussed, the value of  $C_n^2$  is of the order of  $10^{-13} \text{ m}^{-2/3}$ . In this range the optical turbulence can be characterized as Strong Turbulence over link range of 100 m.

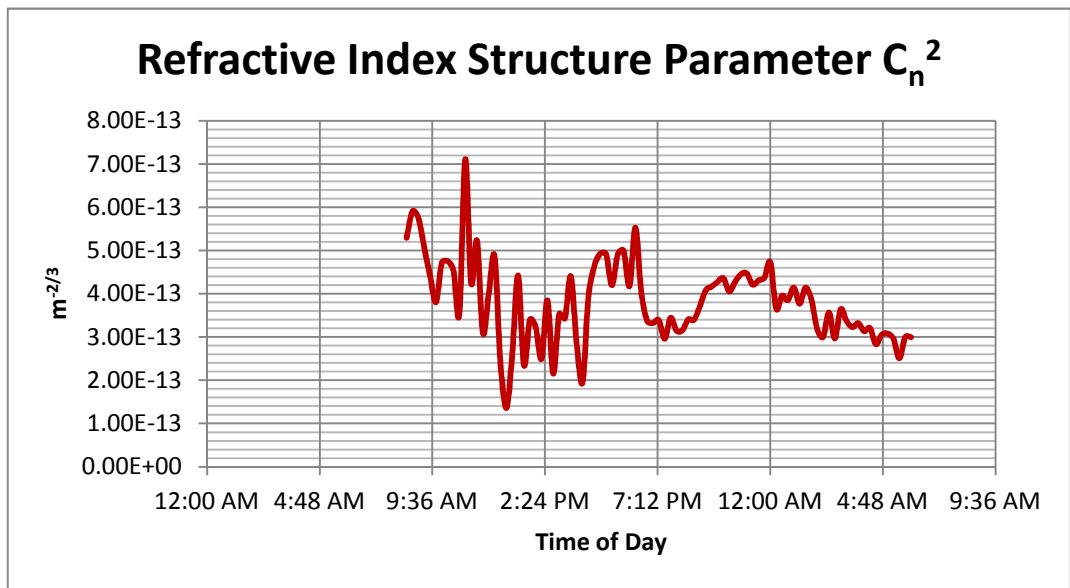


Figure 5.27: Refractive Index Structure Parameter

**5.14.7 Comparative Effect of Atmospheric Optical Turbulence in terms of Variance at a link Range of 1 Km distance** When the link range is extended from 100 m to 1000 m, clear analysis based on the exiting Rytov Variance Model (refer para 5.12.3) indicates that the Receiver would experience very Strong Fluctuations ranging from  $\sigma_R^2 = 10 - 55$ . In order to reduce these effects considerably at such high distances, we would need to increase the aperture diameter of the receiver. At such high link ranges, use of non imaging optics like scattering plates would be more advantageous to counter signal fluctuations due to very strong turbulence.

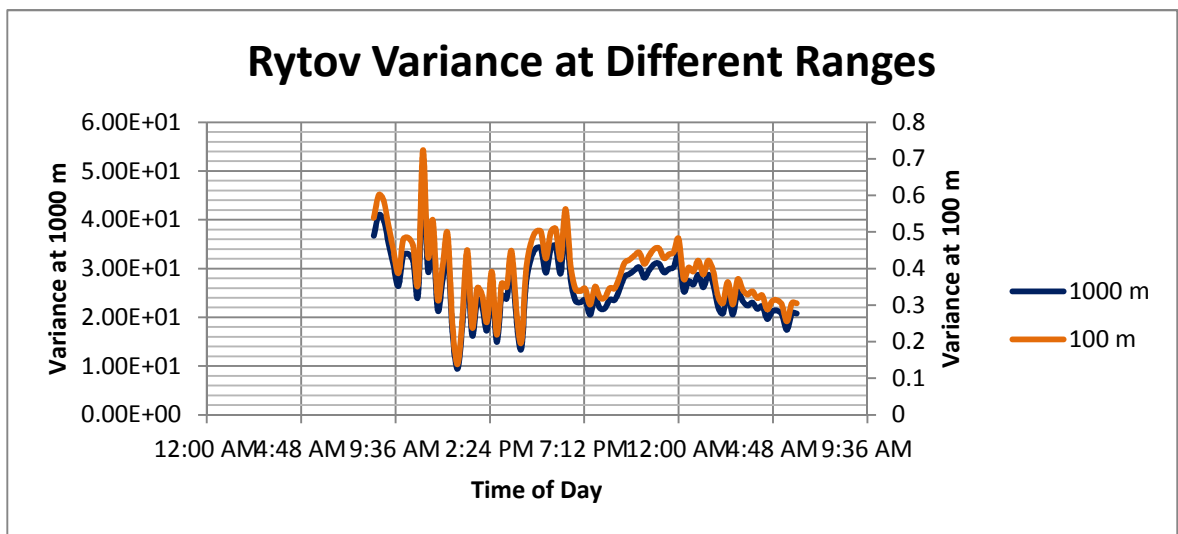


Figure 5.28: Rytov Variance expected at 1 Km FSO Link Range

### 5.15 Quantifying Angle of Arrival Fluctuations – FSO Link Range 100 m

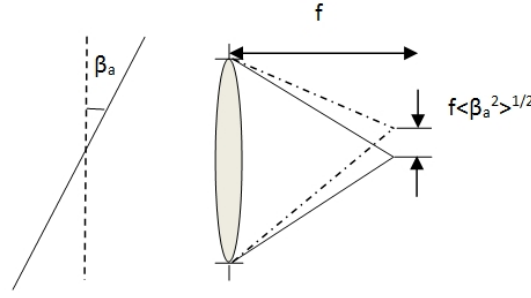


Figure 5.29: Angle of Arrival and Image Jitter

Angle of arrival fluctuations of an optical wave in the plane of the Receiver aperture are associated with image jitter (dancing) on the focal plane of any imaging system. Fluctuations in the angle of arrival,  $\beta_a$  are described in terms of phase structure function [8].

Let  $\Delta S$  denote the total phase shift across a collecting Lens of diameter  $2W_G$  and  $\Delta l$  the corresponding optical path difference. These quantities are related by

$$k\Delta l = \Delta S$$

Assuming  $\beta_a \ll 0$ ,  $\sin \beta_a \approx \beta_a$

$$\beta_a = \frac{\Delta l}{2W_G} = \frac{\Delta S}{2kW_G}$$

Assuming mean  $\langle \beta_a \rangle = 0$ , variance of angle of arrival

$$\langle \beta_a \rangle^2 = \frac{\langle (\Delta S)^2 \rangle}{(2kW_G)^2}$$

It is mathematically found that **Root mean square (rms) angle of arrival** is defined as

$$\sqrt{\langle \beta_a^2 \rangle} = \sqrt{2.91 C_n^2 L (2W_G)^{-\frac{1}{3}}}, \quad 2W_G \gg l_0$$

Also, image jitter takes place on the focal plane of the system [8]. The **rms image displacement** is defined as the angle of arrival multiplied by focal length ‘f’ of the collecting lens of the receiver

$$rms \text{ image jitter} = f \langle \beta_a^2 \rangle^{1/2} = f \sqrt{2.91 C_n^2 L (2W_G)^{-\frac{1}{3}}}, \quad 2W_G \gg l_0$$

From experimental calculations,  $C_n^2 \sim 10^{-13} \text{ m}^{-2/3}$ ,  $2W_G = 50 \text{ mm}$ ,  $L = 100 \text{ m}$

Hence,

$$\text{rms angle of arrival, } \langle \beta_a^2 \rangle^{1/2} = (2.91 \times 10^{-13} \times 100 \times (50 \times 10^{-3})^{-1/3})^{1/2} = \mathbf{8.8876 \mu rad} \text{ (Approx)}$$

$$\text{rms image jitter, } f \langle \beta_a^2 \rangle^{1/2} = 17 \times 10^{-3} \times (2.91 \times 10^{-13} \times 100 \times (50 \times 10^{-3})^{-1/3})^{1/2} = \mathbf{0.15108 \mu m} \text{ (Approx)}$$

*Extending discussion for  $L = 1 \text{ Km}$ , under existing experimental conditions,*

$$\text{rms angle of arrival, } \langle \beta_a^2 \rangle^{1/2} = (2.91 \times 10^{-13} \times 1000 \times (50 \times 10^{-3})^{-1/3})^{1/2} = \mathbf{28.105 \mu rad} \text{ (Approx)}$$

$$\text{rms image jitter, } f \langle \beta_a^2 \rangle^{1/2} = 17 \times 10^{-3} \times (2.91 \times 10^{-13} \times 1000 \times (50 \times 10^{-3})^{-1/3})^{1/2} = \mathbf{0.4778 \mu m} \text{ (Approx)}$$

While developing an FSO system over greater link ranges, affected by channel under strong Atmospheric Turbulence conditions, if we use imaging optics at the receiver end, the receiver, while receiving transmit data is bound to encounter image jitters (order of  $\sim \mu m$ ) which would have considerable effect on performance of the FSO Link and would increase the Probability of Fade for any defined threshold value  $I_T$ . These image jitters are based on angle of arrival of the beam at plane of receiver optics. Change in angle of arrival (order of  $\sim \mu rad$ ) is affected by instantaneous turbulence effects in the channel, which result in beam sway while travelling along the channel (Figure 5.29). Image jitter can be effectively mitigated by employing Non imaging Optics instead of Imaging Optics at the receiver end. (Further discussed in para 5.18)

### **5.16 Quantifying Beam Wander – FSO Link Range 100 m**

The far field angular spread of a free space propagating laser beam of diameter  $2W_0$  is of the order of  $\lambda/2W_0$ . In the presence of optical turbulence, however, a finite, optical beam will experience random deviations as it propagates, causing further spreading by large scale inhomogeneities of the atmosphere. Over short intervals, the beam profile at the receiver randomly moves off the boresight and in doing so can become highly skewed from existing Gaussian profile [8].

The instantaneous center of the beam (Hot Spot) is therefore randomly displaced in the receiver plane, producing **Beam Wander**. This phenomenon is characterised statistically by the variance of the Hot Spot displacement along an axis or by variance of magnitude of Hot Spot Displacement. Beam wander essentially has a time constant on the order of (beam diameter)/(wind speed)

**General Model for Beam Wander** Beam wander at the receiver plane can be modeled as if it arises from a random tilt angle at the transmitter plane.

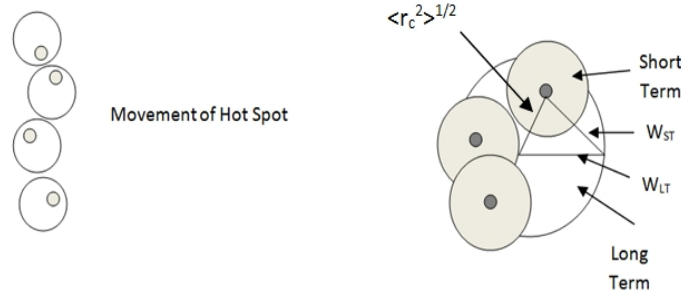


Figure 5.30: Beam Wander

The movement of short term beam depicted by the shaded circular regions in figure 5.30 leads to the larger outer circle over a long time period, which is referred to as long term spot size  $W_{LT}$ .

Analytic expression [8] for variance of beam wander fluctuations is given by

$$W_{LT}^2 = W^2(1 + T) = W^2(1 + 1.33\sigma_R^2\Lambda^{5/6})$$

Here,  $W_{LT}$  represents the long term spot size which is a result of Beam Wander, Beam Breathing and Diffraction.

$$W_{LT}^2 = W^2 + W^2T_{SS} + W^2T_{LS}$$

$T = T_{SS} + T_{LS}$ , where,

$W^2$  is due to pure diffraction beam spreading

$W^2T_{SS}$  is due small scale beam spread as a result of beam breathing and short term beam radius  $W_{ST}$

$W^2T_{LS}$  is due Beam Wander, or the variance of instantaneous center of the beam in receiver plane ( $z=L$ )

For a collimated beam,

rms Beam Wander Displacement [8] is analytically defined as

$$\sqrt{\langle r_c \rangle^2} = \sqrt{2.42C_n^2 L^3 W_0^{-1/3}}$$

From experimental calculations,  $C_n^2 \sim 10^{-13} \text{ m}^{-2/3}$ ,  $L = 100 \text{ m}$ ,  $W_0 = 0.10046 \text{ mm}$  (Beam Radius, as established in Para 5.4)

Hence,  $\langle r_c \rangle = 0.00228 \text{ m} = 0.228 \text{ cm} = 2.28 \text{ mm}$

Effective Long term Beam Spot size [8] (For collimated Beam),

$$W_{LT} = W(1 + 1.33\sigma_R^2 \Lambda^{5/6})^{1/2}$$

From experimental calculations,  $L = 100 \text{ m}$ ,  $W = 170 \text{ mm}$  (Beam Radius at Receiver Plane, refer para 5.4 ( $L = 100 \text{ m}$ ),  $\sigma_R^2 \approx 0.5$ ,  $k$  (wave number)  $= 2\pi/\lambda = 11.81 \times 10^6$  (For  $\lambda = 531.8 \text{ nm}$ )

Also,

$$\Lambda = \frac{2L}{kW^2} = 2 \times 100 / (11.81 \times 10^6 \times (170 \times 10^{-3})^2) = 585.979 \times 10^{-6}$$

$$W_{LT} = 170 \times 10^{-3} (1 + (1.33 \times 0.5 \times (585.979 \times 10^{-6})^{5/6}))^{1/2}$$

$$\mathbf{W_{LT} = 170.114 \text{ mm}}$$

Also, Effective Short term Beam Spot Size [8] (For collimated Beam),

$$W_{ST} = W \sqrt{(1 + 1.33\sigma_R^2 \Lambda^{5/6}) \left[ 1 - 0.66 \left( \frac{\Lambda_0^2}{1 + \Lambda_0^2} \right)^{1/6} \right]}$$

Again,

From experimental calculations,  $L = 100 \text{ m}$ ,  $W_0 = 0.10046 \text{ mm}$  (Beam Waist,  $\sigma_R^2 \approx 0.5$ ,  $k$  (wave number)  $= 2\pi/\lambda = 11.81 \times 10^6$  (For  $\lambda = 531.8 \text{ nm}$ )

$$\Lambda_0 = \frac{2L}{kW_0^2} = 2 \times 100 / (11.81 \times 10^6 \times (0.10046 \times 10^{-3})^2) = 1678.007$$

$$\begin{aligned} W_{ST} &= 170 \times 10^{-3} (1 + (1.33 \times 0.5 \times (585.979 \times 10^{-6})^{5/6}) [1 - 0.66 ((1678.007)^2 / (1 + (1678.007)^2))^{1/6}])^{1/2} \\ &= 170 \times 10^{-3} \times ((1.0001347) \times [0.34])^{1/2} \end{aligned}$$

$$\mathbf{W_{ST} = 99.192 \text{ mm}}$$

Hence, in order to reduce the effects of Beam wander at 100m and carrying out effective aperture averaging, calculations suggest that the telescope aperture should be designed having



Aperture diameter 340 mm ( $2W_{LT}$ ), so that at no point of time the beam strays away from the receiver aperture and signal is always detected at the receiver end.

### 5.16.1 Analyzing Effect of Beam Wander at extended link Range of 1 Km

rms Beam Wander Displacement

$$\sqrt{\langle r_c \rangle^2} = \sqrt{2.42 C_n^2 L^3 W_0^{-1/3}}$$

From experimental calculations,  $C_n^2 \sim 10^{-13} \text{ m}^{-2/3}$ ,  $L = 1000 \text{ m}$ ,  $W_0 = 0.10046 \text{ mm}$  (Beam Radius)

Hence,  $\langle r_c \rangle = 0.0228 \text{ m} = 2.28 \text{ cm} = 22.8 \text{ mm}$

Effective Long term Beam Spot size (For collimated Beam),

$$W_{LT} = W(1 + 1.33\sigma_R^2 \Lambda^{5/6})^{1/2}$$

From experimental calculations above,  $L = 1000 \text{ m}$ ,  $W = 1.6929 \text{ m}$  (Beam Radius expected at Receiver Plane, ( $L = 1000 \text{ m}$ ) (Refer Para 5.4),  $\sigma_R^2 \approx 55$  (Highest value of Rytov variance based on strong turbulence at  $L=1000 \text{ m}$  (Refer para 5.14.7)),  $k$  (wave number)  $= 2\pi/\lambda = 11.81 \times 10^6$  (For  $\lambda = 531.8 \text{ nm}$ )

Also,

$$\Lambda = \frac{2L}{kW^2} = 2 \times 1000 / (11.81 \times 10^6 \times (1.6929)^2) = 59.09 \times 10^{-6}$$

$$W_{LT} = 1.6929 (1 + (1.33 \times 55 \times (59.09 \times 10^{-6})^{5/6}))^{1/2}$$

$$W_{LT} = 1.7113 \text{ m}$$

Also, Effective Short term Beam Spot Size (For collimated Beam),

$$W_{ST} = W \sqrt{(1 + 1.33\sigma_R^2 \Lambda^{5/6}) \left[ 1 - 0.66 \left( \frac{\Lambda_0^2}{1 + \Lambda_0^2} \right)^{1/6} \right]}$$

Again,

From experimental calculations,  $L = 1000 \text{ m}$ ,  $W_0 = 0.10046 \text{ mm}$  (Beam Waist,  $\sigma_R^2 \approx 55$ ,  $W = 1.6929 \text{ m}$ , ( $k$  (wave number)  $= 2\pi/\lambda = 11.81 \times 10^6$  (For  $\lambda = 531.8 \text{ nm}$ ))

$$A_0 = \frac{2L}{kW_0^2} = 2 \times 1000 / (11.81 \times 10^6 \times (0.10046 \times 10^{-3})^2) = 16780.07$$

$$W_{ST} = 1.6929 (1 + (1.33 \times 55 \times (59.09 \times 10^{-6})^{5/6}) [1 - 0.66 ((16780.07)^2 / (1 + (16780.07)^2))^{1/6}])^{1/2}$$

$$= 1.6929 \times ((1.0219) \times [0.34])^{1/2}$$

$$W_{ST} = 0.9978 \text{ m}$$

In order to reduce the effects of Beam wander at 1000m and carrying out effective aperture averaging, calculations suggest that the telescope aperture should be designed having Aperture diameter 3.423 m ( $2W_{LT}$ ), so that at no point of time the beam strays away from the receiver aperture and signal is always detected at the receiver end.

### 5.16.2 Experimental Quantification of Beam Wander at Link Range 60m

Effect of beam wander can be suitably determined by transmitting a high power, highly collimated Laser Beam onto the receiver end in order to allow photo-detector to operate in highly Non Linear / saturated regime. When the photo-detector operates in non linear regime, random effects of index of refractive turbulence (order of  $\mu\text{sec}$ ) are not picked up by the photo-detector, thereby reducing any kind of change in variance of transmitted data to zero. However, if the Beam wanders from its defined course over any particular interval, there is a drastic increase in variance of received data as is clearly brought out in figure 5.31, depicting analysis of data transmitted over a 24 hour cycle at a link range of 60 m while allowing the photo-detector to be operated in non linear regime. Such arrangement is highly beneficial to record precise intervals of beam wander which may arise due to temporary misalignments of the link or any kind of seismic activity leading to building sway.

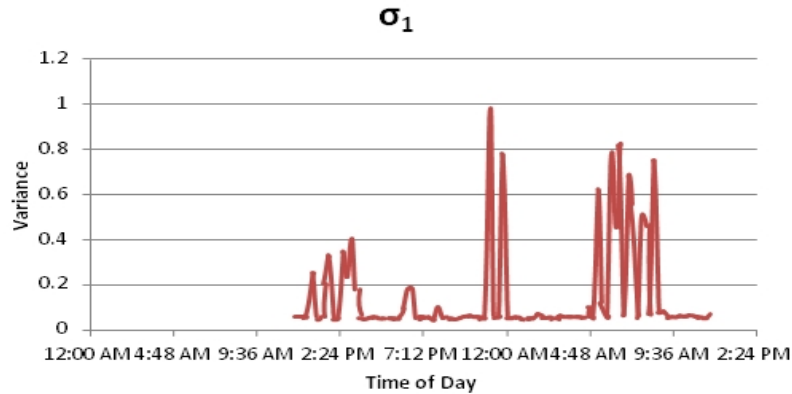


Figure 5.31: Variance due to Beam Wander- FSO Link 60 m

**5.17 Estimating Probability of Fade** Probability of fade describes the percentage of time the irradiance of the received wave is below some prescribed threshold value  $I_T$  [8].

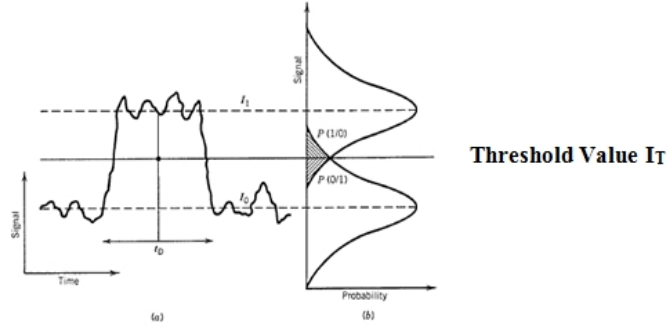


Figure 5.32: Fluctuating signal generated at the Receiver

In order to compute probability of fade, Fade threshold parameter  $F_T$ , given in decibels (dB), represents the dB level below the on-axis mean irradiance that the threshold  $I_T$  is set.

$$F_T(\text{dB}) = 10 \log_{10} \left( \frac{\langle I(0, L) \rangle}{I_T} \right)$$

Probability of fade for the 100 m FSO Link (divergent, low power), was computed based on the experimental data collected over a 24 hour cycle. While computing Probability of Fade, mean value of received intensity was calculated based on the entire range of data collected over a 24 Hour cycle when '1' was transmitted. We vary the fade threshold Parameter  $F_T$  given in decibels (dB) from -3 to 10 at intervals of 0.5 dB and compute the corresponding threshold  $I_T$  based on above equation.

In order to compute probability of Fade at any particular threshold, the entire experimental data is scanned in order to ascertain the total number of data values which are less than the corresponding threshold Level.

$$\text{Fade Probability, } P_r(I \leq I_T) = \frac{\text{No. of data values below threshold Level } I_T}{\text{Total No. of Data values collected over a 24 Hr cycle}}$$

Figure 5.33 brings out that if the threshold level is set at the mean value of the data collected, probability of Fade is extremely high (0.8). Fade Probability reduces to  $10^{-3}$  when threshold value  $I_T$  is set 8 dB below mean value of data collected.

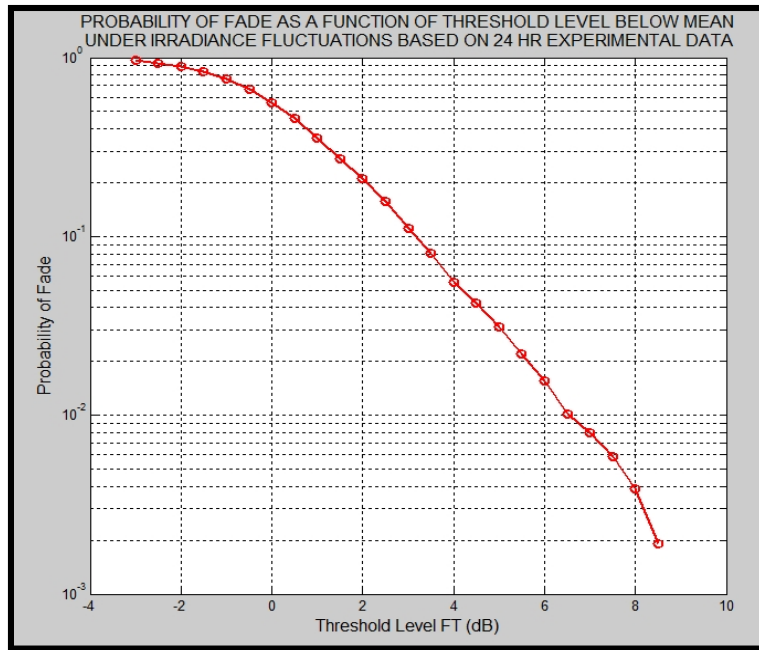


Figure 5.33: Probability of Fade as a Function of Fade Parameter

### 5.18 Non Imaging Optics

At very high link ranges, presence of beam divergence at source (even if the beam is highly collimated) leads to very large beam spot size at the receiver aperture. It may not be feasible to accommodate telescope apertures of such large diameters at receiver end. More so, it has been clearly analysed that the expected beam fluctuations are going to be very strong at such high link ranges. This may lead to very high fluctuations at the receiver end if we use imaging optical systems based on discussions in para 5.15. In order to capture signal suitably at such large distances, possibility should be explored for use of Non Imaging optics instead of Imaging Optics.

Non imaging optics, such as scattering plates enables optimum transfer of luminous power rather than forming an image [13], [14]. Most vital attribute of such optical systems as compared to their imaging counterparts is their high tolerance towards variations in the relative position of light source and optic which aids as efficient counter to strong beam fluctuations at extended link ranges.

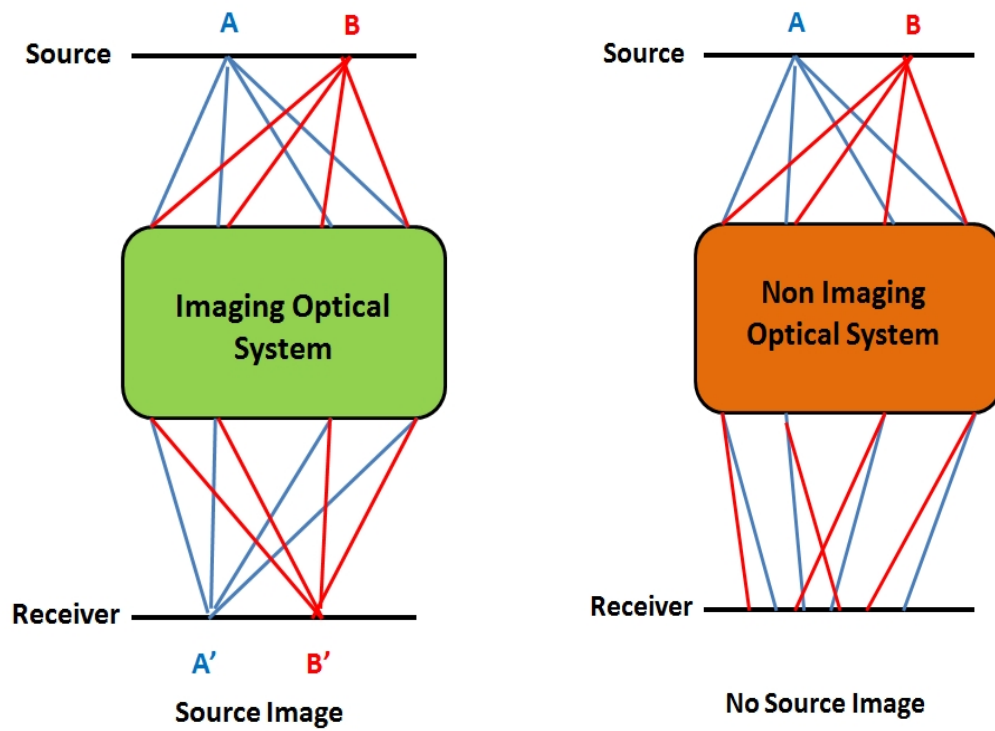


Figure 5.34: Comparison of Imaging and Non Imaging Optical System

## CHAPTER 6

### SUMMARY AND CONCLUSION

During the work undertaken as part of the project, a detailed literature and global market survey was carried out in order to propose an extensive plan in developing a directly modulated, high power, 1550 nm Laser Source capable of operating at ~1% duty cycle having pulse width of 5ns and repetition rate  $> 2.3$  Mbps. Peak power levels achievable by the design are expected to be  $> 40$  W.

As a second requirement of the project an FSO Link was setup at varying ranges upto a maximum link range of 250 m using a commercially available 531.8 nm green Laser pointer source. The optical source was externally modulated by an electronic driver circuit suitably designed to achieve ON-OFF keying modulation at a defined bandwidth. Green Laser source was chosen for the project owing to its ease of availability, high transmittance, narrow beam divergence and very high coherence which enables us to quantify spatial channel effects affecting performance of the FSO link at higher link ranges.

FSO Link was used to experimentally quantify channel effects over 24 hour cycle to include atmospheric extinction comprising of atmospheric attenuation and scattering, atmospheric turbulence leading to scintillation and beam wander, affecting performance of the FSO link at link range of 100 m. Link Bandwidth has been setup to 1.1 MHz in order to quantify any variations due to atmospheric turbulence leading Beam Wander (msec scale) and scintillation ( $\mu$ sec scale).

The effects so quantified have been extrapolated to a link range of 1000 m in order to ascertain their corresponding influence on performance of the Link at such high ranges. It was established that Atmospheric Extinction effects like attenuation and scattering are fairly deterministic in nature, while effects due to atmospheric turbulence such as scintillation and beam wander are stochastic in nature owing to instantaneous atmospheric conditions prevalent based upon geographic location of link, temperature, windspeed and time of day. These effects need to be quantified statistically. Based upon experimental data, fade probability of the Link for a 100 m link range has been established over a 24 hour cycle.

Attenuation due to Atmospheric extinction based on experimental quantification and extrapolation for a Link range of 1 Km is expected to be 39 dB/Km at day time and 34 dB/Km during the night. The experimental results have also been suitably compared and verified with existing theoretical models on the subject.

It was noted that FSO systems based on coherent light sources such as LASER are plagued with Scintillations and Beam Wander as a result of atmospheric turbulence which are primarily random in nature. Quantification of effects of Atmospheric Turbulence was carried over a link range of 100 m and corresponding results were extrapolated to link range of 1 Km. It was established that Rytov variance,  $\sigma_R^2$  at 100 m FSO Link varies between 0.5-0.85 over 24 Hour cycle. However, this variance, when extrapolated to a link range of 1000 m is of the order of  $\sigma_R^2 = 10^{-55}$ . Also, Index of Refractive Turbulence  $C_n^2$  is quantified to be of the order of  $10^{-13} \text{ m}^{-2/3}$ . These values are fairly high to qualify for strong fluctuations at the receiver end for such link ranges.

At very high link ranges, presence of beam divergence at source (even if the beam is highly collimated) leads to very large beam spot size at the receiver aperture. It may not be feasible to accommodate telescope apertures of such large diameters at receiver end. More so, the expected beam fluctuations at such extended ranges are going to be very strong. This may lead to very high fluctuations at the receiver end. Non imaging optics, such as scattering plates enables optimum transfer of luminous power. Most vital attribute of such optical systems as compared to their imaging counterparts is their high tolerance towards variations in the relative position of light source and optic which aids as efficient counter to strong beam fluctuations at extended link ranges. Hence, in order to capture signal suitable at large distances, possibility should be explored for use of Non Imaging optical systems.

It was experimentally verified that when a highly collimated, high power transmit laser beam is allowed to be detected by the optical receiver, it is possible to achieve very efficient communication link with broad eye patterns, thereby dropping the BER to order of  $e^{-200}$ . This re-enforces the fact that a carefully designed FSO system is capable of achieving very high data rates in communication with extremely low probability of error.

FSO Communication system exhibits tremendous scope in wireless transmission standards with reference to defence communication requirements at large. It is an important area of ongoing research and project development in Academia and Industry at a global level both in

military and commercial market. This technology has enormous potential in terms of Bandwidth utilization and comparatively very low setup cost.

From the project, we can envisage a leaner, cost effective, portable and a more reliable means of communication standard which has the capability to bypass enemy Electronic Counter Measures owing to its operation in Optical Domain and extremely low beam divergence of laser source.



# CHAPTER 7

## FUTURE SCOPE

### 7.1 Employing Spatial Diversity Schemes to FSO Link

The performance of FSO communication severely suffers from turbulence-induced fading caused by atmospheric conditions. Multiple laser transmitters and/or receivers can be deployed at both ends to mitigate the turbulence fading and exploit the advantages of spatial diversity. Spatial diversity is particularly crucial for strong turbulence channels in which single-input single-output (SISO) link performs below expectation. When Multiple Input Multiple Output (MIMO) systems are used, we can expect significant diversity / capacity gains based on multiple transmitter/receivers deployment in FSO channels.

### 7.2 MIMO-OFDM based FSO System

At higher bit rates the problem of Inter Symbol Interference (ISI) is predominant. Due to the effect of ISI, the capacity of the MIMO system severely degrades. Orthogonal Frequency Division Multiplexing (OFDM) provides a solution to this problem. In OFDM, the original signal is modulated by orthogonal tones. The entire stream is divided into many parallel substreams. Hence, the symbol duration is increased and the effect of ISI is mitigated. OFDM has high spectral and power efficiency and simple frequency domain equalization. The implementation of OFDM can be easily carried out by using IFFT at the transmitter and FFT at the receiver [15]. Thus, it provides a cost effective solution to combat fading caused due to atmospheric turbulence in FSO transmission. As the signals in optical communication are invariably unipolar in nature, we can either employ DC biased OFDM or clipped OFDM in the optical domain. Thus, the combination MIMO-OFDM FSO provides robustness to the system and is an effective solution for next generation FSO systems.

### 7.3 Exploiting advantages of both RF and FSO Link for establishing communication

It has been established over careful research that RF Link exhibits high performance over a channel affected with Fog. However, performance of the link drops when the channel is affected by rain. FSO Link on the other hand performs comparatively better in rainy environment. Performance of FSO link gets drastically affected at low visibility ranges owing to dense Fog conditions. In order to establish wireless communication at extremely low BER

over a 365 day calendar cycle, advantages of both technologies can be exploited in order to ensure high rate of link availability.

## REFERENCES

1. Free space optical communications: An overview of applications and Technologies - J E Kaufmann - Boston IEEE Comm, 1 Dec 2011.
2. B.E.A Saleh, M.C. Teich, **Fundamentals of Photonics**, Wiley Series, 2<sup>nd</sup> Ed.
3. An Introduction to Free-space Optical Communications - Hennes Henniger, Otakar Wilfert – Radioengineering, Vol. 19, No. 2, June 2010.
4. Light Sources and Laser Safety - F Seeber, **Fundamentals of photonics**, 2007, remotesensing.spiedigitallibrary.org.
5. [http://www.rp-photonics.com/master\\_oscillator\\_fiber\\_amplifier.html](http://www.rp-photonics.com/master_oscillator_fiber_amplifier.html)
6. GP Agarwal, **Fiber-Optic Communication systems**, Wiley Series, 3<sup>rd</sup> Ed.
7. High-power double-clad fiber lasers - L Zenteno, Lightwave Technology Journal, Vol 11, Issue 9, Sep 1993.
8. Larry C Andrews, Ronald L Phillips, **Laser Beam Propagation through Random Media**, SPIE Press, 2<sup>nd</sup> Ed.
9. Dense Maritime Fog Attenuation Prediction from Measured Visibility Data - Farukh Nadeem, Erich Leitgeb – Radioengineering, Vol. 19, No. 2, June 2010.
10. Characterization of Atmospheric Turbulence Effects and their Mitigation Using Wavelet-Based Signal Processing - Latsa B Pedireddi , Balaji Srinivsan - IEEE TRANSACTIONS ON COMMUNICATIONS, VOL. 58, NO. 6, JUNE 2010
11. <http://www.rapidtables.com/calc/light/lux-to-watt-calculator.htm>
12. Light Measurement Handbook © 1998 by Alex Ryer, International Light Inc
13. Lighting by Design - David Pelka – oemagazine, SPIE Newsroom - 31 Aug 2005
14. Roland Winston, Juan C Minano, Pablo Benitez, **Nonimaging Optics**, Elsevier Academic Press
15. David Tse, Pramod Viswanath, **Fundamentals of Wireless Communications**, Cambridge University Press, 2005
16. RK Shevgaonkar, **Fiber Optics**, IIT Bombay
17. Understanding the Performance of Free-Space Optics – LightPointe White Paper Series

**Appx 'A'****Bill of Materials**

<b>Se r No</b>	<b>Item</b>	<b>Nomenclature</b>	<b>Model No.</b>	<b>Quantity</b>	<b>Vendor</b>	<b>Cost Per Item (USD)</b>	<b>Total Cost (USD)</b>	<b>Remarks</b>
1	Laser Seed Driver Assembly	Picolas High Speed Laser Driver	BFS-VRM 03 HP	01	Laser Components	2525	2525	Via formal quotation
2	1550 nm Laser Seed	1550 nm Fabry-Perot Laser Diode	FPL1009S	01	ThorLabs	1639	1639	Via formal quotation
3	980 nm Pump Laser	500 – 700 mW Single Mode Pump Lasers	AC1401-0700- 0980-SM	02	Gooch & Housego	1425	2850	Via email
4	Laser Seed Driver Assembly	OEM Pulsed Laser Diode Driver	Model 763	02	Analog Modules, Inc	896	1792	Via email
5	1550 nm Isolator	1550 nm Isolator (High Power) with connector	ISO-H	04	OeMarket	359	1436	Via Website
6	980 nm Isolator	980 nm Isolator with connector	ISO-S-980/85	02	Oemarket	1600	3200	Via Website
7	95x5 Coupler (1550 nm)	1x2 Single Mode Optical Couper – Dual window 1310 & 1550 nm	DWC1315-1X2- P-95/5-0-SA	02	Oemarket	45	90	Via Website
8	Multimod e Pump Combiner	(2+1)x1 Pump and Signal Combiner	PSC02101001 A	02	DK Photonics Technology Limited	350	700	Via Website
9	Attenuato r	1550 nm Inline Fixed Optical Attenuator	FOA-IL-1550-30- 0-FA	02	OeMarket	20.58	41.16	Via Website
10	LNA	-	-	02	Unilumen Photonics	70	140	-
11	Erbium Doped Fiber	SM Erbium Doped Single Mode Fiber	SM-ESF-7/125	20 mtrs	Nufern	100	2000	Via Website
12	Erbium Yttrium Doped Fiber	CATV Amplifier 6/125 Er:Yb-Doped Double Clad PM Fiber	SM-EYDF-6/125- HE	10 mtrs	Nufern	80	800	Via Website
<b>TOTAL (Approximate amount in USD)</b>							<b>~17213 (USD)</b>	
<b>Approximate Amount in Rupees</b>							<b>Rs 10,64,021.59</b>	

**Quantification of Atmospheric Extinction Effects****Time of Experiment** 1:30 pm - 2:10 pm

Ser No	Distance (m)	Atmospheric Lux	Lux with Green LASER	Lux only because of Green LASER	Optical Power (Rx) (Watts)	Power (dBm)
1	1	13650	174000	160350	0.0207	13.15185
2	2	15170	158500	143330	0.0185	12.66453
3	3	14470	143000	128530	0.0166	12.19121
4	6	12470	108600	96130	0.0124	10.92975
5	9	14310	71600	57290	0.00738	8.68195
6	12	12580	58900	46320	0.00597	7.758847
7	21	11170	44100	32930	0.00424	6.277079
8	42	11110	12690	1580	0.000203	-6.91227
9	63	3830	4720	890	0.000115	-9.40494
10	84	4930	5580	650	0.0000837	-10.7697
11	100	4970	5240	270	0.0000348	-14.5852
12	150	4940	5182	242	0.0000307	-15.134
13	200	4830	5032	202	0.0000257	-15.897
14	250	4750	4929	179	0.0000228	-16.414

Table 1: Experimental Quantification of Atmospheric Attenuation – Day Time

**Time of Experiment** 6:35 pm - 6:45 pm

Ser No	Distance (m)	Atmospheric Lux	Lux with Green LASER	Lux only because of Green LASER	Optical Power (Rx) (Watts)	Power (dBm)
1	1	0	135000	135000	0.0174	12.4045
2	2	0	95000	95000	0.0122	10.8784
3	3	0	45600	45600	0.00588	7.69081
4	6	0	35700	35700	0.00460	6.627844
5	9	0	25600	25600	0.003299	5.183561
6	12	0	20500	20500	0.002642	4.2187
7	21	0	18700	18700	0.002409	3.819578
8	42	0	4630	4630	0.000597	-2.24303
9	63	0	2760	2760	0.0003556	-4.48975
10	84	0	1265	1265	0.000163	-7.87793
11	100	0	322	322	0.0000415	-13.8203
12	150	0	290	290	0.00003685	-14.335
13	200	0	232	232	0.00002953	-15.297
14	250	0	207	207	0.00002639	-15.785

Table 2: Experimental Quantification of Atmospheric Attenuation – Night Time

Time of Experiment: 0500 Hrs

Visibility: 350 m

Temperature: 18.1°C

Humidity: 80%

Ser No	Distance (m)	Atmospheric Lux	Lux with Green LASER	Lux only because of Green LASER	Optical Power (Rx) (Watts)	Power (dBm)
1	1	0	159300	159300	0.020239856	-16.9379
2	2	0	103400	103400	0.013137483	-18.8149
3	3	0	97000	97000	0.012324331	-19.0924
4	6	0	78000	78000	0.009910287	-20.0391
5	9	0	5600	5600	0.000711508	-31.4782
6	12	0	4700	4700	0.000597158	-32.2391
7	18	0	2310	2310	0.000293497	-35.324
8	21	0	1618	1618	0.000205575	-36.8703
9	42	0	960	960	0.000121973	-39.1374
10	63	0	420	420	5.33631E-05	-42.7276
11	84	0	133	133	1.68983E-05	-47.7216
12	100	0	71	71	9.0209E-06	-50.4475

Table 3: Experimental Quantification of Atmospheric Extinction, Moderate Fog Conditions

**Appx 'C'**

### Experimental Quantification and Analysis of Atmospheric Turbulence based on Histogram Plot over 24 Hour cycle

Ser No	Time	Temperature (°C)	Wind Speed (Kmph)	I <sub>1</sub> (V)	I <sub>0</sub> (V)	σ <sub>0</sub> <sup>2</sup>	σ <sub>1</sub> <sup>2</sup>	σ <sub>0</sub>	σ <sub>1</sub>	C <sub>n</sub> <sup>2</sup>	σ <sub>1</sub> <sup>2</sup> , 1 Km
1	8:30 AM	32.2	14	2.176	-0.04325	0.02978	0.5389	0.172569	0.734098	5.30E-13	3.67E+01
2	8:45 AM	32.1	14	1.765	-0.03802	0.02795	0.6009	0.167183	0.775177	5.91E-13	4.09E+01
3	9:00 AM	32.2	14	1.801	-0.04	0.02771	0.5863	0.166463	0.765702	5.76E-13	3.99E+01
4	9:15 AM	32.3	14	1.732	-0.03936	0.02826	0.5161	0.168107	0.718401	5.07E-13	3.52E+01
5	9:30 AM	33	14	2.334	-0.03953	0.02873	0.4494	0.169499	0.670373	4.42E-13	3.06E+01
6	9:45 AM	33.7	14	2.395	-0.05372	0.04323	0.3874	0.207918	0.622415	3.81E-13	2.64E+01
7	10:00 AM	34.7	16	2.294	-0.05403	0.0438	0.4801	0.209284	0.692892	4.72E-13	3.27E+01
8	10:15 AM	34.6	16	1.766	-0.05517	0.04338	0.4841	0.208279	0.695773	4.76E-13	3.30E+01
9	10:30 AM	35.2	16	1.95	-0.03043	0.02856	0.4611	0.168997	0.679043	4.53E-13	3.14E+01
10	10:45 AM	34.6	16	2.297	-0.03872	0.02776	0.36	0.166613	0.6	3.54E-13	2.45E+01
11	11:00 AM	34.1	18	1.683	-0.03544	0.02905	0.7233	0.170441	0.85047	7.11E-13	4.93E+01
12	11:15 AM	35.3	18	1.56	-0.03627	0.02954	0.4333	0.171872	0.658255	4.26E-13	2.95E+01
13	11:30 AM	34.5	18	1.663	-0.04203	0.02989	0.5317	0.172887	0.729178	5.23E-13	3.62E+01
14	11:45 AM	36.4	18	0.9975	-0.04334	0.02654	0.3151	0.162911	0.561338	3.10E-13	2.15E+01
15	12:00 PM	38.4	18	0.7634	-0.04295	0.02699	0.4065	0.164286	0.637574	4.00E-13	2.77E+01
16	12:15 PM	38.8	18	0.8593	-0.04537	0.0271	0.4954	0.164621	0.703847	4.87E-13	3.38E+01
17	12:30 PM	40	18	0.5789	-0.04637	0.0272	0.2446	0.164924	0.494571	2.40E-13	1.67E+01
18	12:45 PM	40.6	18	0.4459	-0.04537	0.02666	0.1383	0.163279	0.371887	1.36E-13	9.42E+00
19	1:00 PM	38.5	22	0.5624	-0.05354	0.02611	0.2632	0.161586	0.51303	2.59E-13	1.79E+01
20	1:15 PM	40.9	22	1.09	-0.05508	0.02823	0.4504	0.168018	0.671118	4.43E-13	3.07E+01
21	1:30 PM	39.2	22	0.5849	-0.05747	0.0263	0.2392	0.162173	0.489081	2.35E-13	1.63E+01
22	1:45 PM	38.2	22	0.6572	-0.05892	0.02657	0.345	0.163003	0.587367	3.39E-13	2.35E+01
23	2:00 PM	41.1	22	0.7104	-0.05364	0.02589	0.3289	0.160904	0.573498	3.23E-13	2.24E+01
24	2:15 PM	38.8	22	0.7239	-0.05359	0.02653	0.254	0.16288	0.503984	2.50E-13	1.73E+01

Ser No	Time	Temperature (°C)	Wind Speed (Kmph)	I <sub>1</sub> (V)	I <sub>0</sub> (V)	$\sigma_0^2$	$\sigma_1^2$	$\sigma_0$	$\sigma_1$	$C_n^2$	$\sigma_1^2, 1\text{ Km}$
25	2:30 PM	44.3	22	1.128	-0.0417	0.02821	0.3916	0.167958	0.62578	3.85E-13	2.67E+01
26	2:45 PM	40.3	22	0.571	-0.05245	0.02647	0.2194	0.162696	0.468402	2.16E-13	1.49E+01
27	3:00 PM	41.2	14	0.5248	-0.05075	0.02571	0.3587	0.160343	0.598916	3.53E-13	2.44E+01
28	3:15 PM	41.5	14	0.8628	-0.05058	0.02687	0.3494	0.163921	0.591101	3.43E-13	2.38E+01
29	3:30 PM	40.1	14	0.9878	-0.0503	0.02774	0.4482	0.166553	0.669477	4.41E-13	3.05E+01
30	3:45 PM	41.4	14	0.7832	-0.05043	0.02687	0.2881	0.163921	0.536749	2.83E-13	1.96E+01
31	4:00 PM	40.5	18	0.3981	-0.04937	0.0266	0.1988	0.163095	0.44587	1.95E-13	1.35E+01
32	4:15 PM	39.8	18	1.163	-0.0454	0.0278	0.3998	0.166733	0.632297	3.93E-13	2.72E+01
33	4:30 PM	41.5	18	1.109	-0.04528	0.02769	0.472	0.166403	0.687023	4.64E-13	3.22E+01
34	4:45 PM	39.9	18	1.636	-0.05233	0.02912	0.5013	0.170646	0.708025	4.93E-13	3.42E+01
35	5:00 PM	38.4	18	1.525	-0.05423	0.02824	0.5004	0.168048	0.70739	4.92E-13	3.41E+01
36	5:15 PM	38.1	18	1.465	-0.0503	0.02827	0.4275	0.168137	0.653835	4.20E-13	2.91E+01
37	5:30 PM	38.4	18	1.37	-0.05135	0.02833	0.4998	0.168315	0.706965	4.91E-13	3.41E+01
38	5:45 PM	36.4	18	1.412	-0.05148	0.02858	0.5078	0.169056	0.712601	4.99E-13	3.46E+01
39	6:00 PM	34.1	14	1.268	-0.05348	0.02796	0.4252	0.167212	0.652074	4.18E-13	2.90E+01
40	6:15 PM	30.5	14	1.342	-0.05683	0.02811	0.5625	0.16766	0.75	5.53E-13	3.83E+01
41	6:30 PM	29.5	14	1.15	-0.05591	0.0267	0.412	0.163401	0.641872	4.05E-13	2.81E+01
42	6:45 PM	28.9	14	0.8792	-0.06034	0.02683	0.3436	0.163799	0.586174	3.38E-13	2.34E+01
43	7:00 PM	28.7	14	0.9794	-0.06165	0.0268	0.3383	0.163707	0.581636	3.33E-13	2.30E+01
44	7:15 PM	28.6	14	0.8159	-0.06233	0.02737	0.3446	0.165439	0.587026	3.39E-13	2.35E+01
45	7:30 PM	28.6	14	0.6604	-0.0573	0.0259	0.3013	0.160935	0.548908	2.96E-13	2.05E+01
46	7:45 PM	28.4	14	0.8999	-0.05947	0.02695	0.3507	0.164165	0.592199	3.45E-13	2.39E+01
47	8:00 PM	28.2	14	0.9057	-0.05267	0.02735	0.3207	0.165378	0.566304	3.15E-13	2.18E+01
48	8:15 PM	28	14	1.102	-0.05004	0.02673	0.3209	0.163493	0.56648	3.15E-13	2.19E+01
49	8:30 PM	28	14	1.146	-0.05147	0.02662	0.3466	0.163156	0.588727	3.41E-13	2.36E+01
50	8:45 PM	28.1	14	1.236	-0.04902	0.02637	0.3462	0.162388	0.588388	3.40E-13	2.36E+01
51	9:00 PM	28.1	14	1.248	-0.04954	0.02551	0.378	0.159719	0.614817	3.72E-13	2.58E+01
52	9:15 PM	27.9	14	1.357	-0.05394	0.02746	0.4155	0.165711	0.644593	4.08E-13	2.83E+01



Ser No	Time	Temperature (°C)	Wind Speed (Kmph)	I <sub>1</sub> (V)	I <sub>0</sub> (V)	$\sigma_0^2$	$\sigma_1^2$	$\sigma_0$	$\sigma_1$	C <sub>n</sub> <sup>2</sup>	$\sigma_1^2, 1 \text{ Km}$
53	9:30 PM	28.5	14	1.327	-0.06101	0.0269	0.4239	0.164012	0.651076	4.17E-13	2.89E+01
54	9:45 PM	28.2	14	1.367	-0.05474	0.02669	0.4352	0.163371	0.659697	4.28E-13	2.96E+01
55	10:00 PM	28.3	14	1.334	-0.05471	0.02728	0.4437	0.165167	0.666108	4.36E-13	3.02E+01
56	10:15 PM	28.4	14	1.251	-0.05387	0.02659	0.4127	0.163064	0.642417	4.06E-13	2.81E+01
57	10:30 PM	28.2	14	1.292	-0.05504	0.02599	0.4349	0.161214	0.659469	4.27E-13	2.96E+01
58	10:45 PM	28.1	14	1.292	-0.05493	0.02694	0.4532	0.164134	0.673201	4.45E-13	3.09E+01
59	11:00 PM	28	14	1.326	-0.05114	0.02753	0.4548	0.165922	0.674389	4.47E-13	3.10E+01
60	11:15 PM	27.8	14	1.315	-0.0506	0.027	0.4285	0.164317	0.654599	4.21E-13	2.92E+01
61	11:30 PM	27.8	14	1.316	-0.0475	0.02701	0.4387	0.164347	0.662344	4.31E-13	2.99E+01
62	11:45 PM	27.7	14	1.208	-0.04992	0.02668	0.445	0.16334	0.667083	4.37E-13	3.03E+01
63	12:00 AM	27.4	14	1.177	-0.04814	0.02647	0.4812	0.162696	0.693686	4.73E-13	3.28E+01
64	12:15 AM	27.2	14	1.056	-0.04253	0.02535	0.3724	0.159217	0.610246	3.66E-13	2.54E+01
65	12:30 AM	27.4	14	1.132	-0.04243	0.02497	0.4024	0.158019	0.63435	3.96E-13	2.74E+01
66	12:45 AM	27.4	14	1.09	-0.04276	0.02534	0.3923	0.159185	0.626339	3.86E-13	2.67E+01
67	1:00 AM	27.4	11	0.9853	-0.0435	0.02571	0.4218	0.160343	0.649461	4.15E-13	2.87E+01
68	1:15 AM	27.4	11	1.175	-0.04232	0.02564	0.3837	0.160125	0.619435	3.77E-13	2.61E+01
69	1:30 AM	27.3	11	1.139	-0.0425	0.02569	0.4216	0.160281	0.649307	4.14E-13	2.87E+01
70	1:45 AM	27.2	11	1.101	-0.04366	0.02489	0.3942	0.157766	0.627853	3.87E-13	2.69E+01
71	2:00 AM	26.9	11	0.963	-0.04584	0.0263	0.3241	0.162173	0.569298	3.19E-13	2.21E+01
72	2:15 AM	26.9	11	0.9665	-0.05263	0.02607	0.3054	0.161462	0.55263	3.00E-13	2.08E+01
73	2:30 AM	26.8	11	0.9949	-0.04091	0.02539	0.3631	0.159342	0.602578	3.57E-13	2.47E+01
74	2:45 AM	26.5	11	1.076	-0.03822	0.02627	0.3019	0.16208	0.549454	2.97E-13	2.06E+01
75	3:00 AM	26.6	5	0.9789	-0.03973	0.02561	0.3707	0.160031	0.608851	3.64E-13	2.53E+01
76	3:15 AM	26.7	5	0.9968	-0.03958	0.02628	0.3428	0.162111	0.585491	3.37E-13	2.34E+01
77	3:30 AM	26.8	5	0.973	-0.03866	0.0254	0.3287	0.159374	0.573324	3.23E-13	2.24E+01
78	3:45 AM	27	5	0.855	-0.03696	0.02565	0.3378	0.160156	0.581206	3.32E-13	2.30E+01
79	4:00 AM	27.1	5	0.9521	-0.03708	0.02652	0.319	0.16285	0.564801	3.14E-13	2.17E+01
80	4:15 AM	26.7	5	0.9095	-0.03854	0.02571	0.3265	0.160343	0.571402	3.21E-13	2.22E+01

Ser No	Time	Temperature (°C)	Wind Speed (Kmph)	I <sub>1</sub> (V)	I <sub>0</sub> (V)	$\sigma_0^2$	$\sigma_1^2$	$\sigma_0$	$\sigma_1$	C <sub>n</sub> <sup>2</sup>	$\sigma_1^2, 1 \text{ Km}$
81	4:30 AM	26.6	5	0.8964	-0.03813	0.02687	0.2884	0.163921	0.537029	2.83E-13	1.96E+01
82	4:45 AM	26.3	5	0.7662	-0.03758	0.02485	0.3109	0.157639	0.557584	3.06E-13	2.12E+01
83	5:00 AM	26.5	5	0.8014	-0.03828	0.02531	0.3136	0.159091	0.56	3.08E-13	2.14E+01
84	5:15 AM	26.2	5	0.842	-0.03732	0.02593	0.3011	0.161028	0.548726	2.96E-13	2.05E+01
85	5:30 AM	26.5	5	0.7341	-0.03808	0.02534	0.2555	0.159185	0.50547	2.51E-13	1.74E+01
86	5:45 AM	26.4	5	0.7611	-0.0407	0.02534	0.305	0.159185	0.552268	3.00E-13	2.08E+01
87	6:00 AM	26.4	5	0.7611	-0.0407	0.02534	0.305	0.159185	0.552268	3.00E-13	2.08E+01